AUTOMATIC ISOCHORIC APPARATUS FOR PVT AND PHASE EQUILIBRIUM STUDIES OF NATURAL GAS MIXTURES

A Dissertation

by

JINGJUN ZHOU

Submitted to the Office of Graduate Studies of
Texas A&M University
in partial fulfillment of the requirements for the degree of

DOCTOR OF PHILOSOPHY

May 2005

Major Subject: Chemical Engineering

AUTOMATIC ISOCHORIC APPARATUS FOR PVT AND PHASE EQUILIBRIUM STUDIES OF NATURAL GAS MIXTURES

A Dissertation

by

JINGJUN ZHOU

Submitted to Texas A&M University
in partial fulfillment of the requirements
for the degree of

DOCTOR OF PHILOSOPHY

Approved as to style and content by:

Kenneth R. Hall (Co-Chair of Committee)	James C. Holste (Co-Chair of Committee)
Philip T. Eubank (Member)	Donald G. Naugle (Member)
Kenneth R. Hall (Head of Department)	

May 2005

Major Subject: Chemical Engineering

ABSTRACT

Automatic Isochoric Apparatus for PVT and Phase Equilibrium Studies of Natural Gas Mixtures. (May 2005)

Jingjun Zhou, B.S., Zhejiang University;

M.S., Zhejiang University

Co-Chairs of Advisory Committee: Dr. Kenneth R. Hall
Dr. James C. Holste

We have developed a new automatic apparatus for the measurement of the phase equilibrium and *pVT* properties of natural gas mixtures in our laboratory. Based on the isochoric method, the apparatus can operate at temperature from 200 K to 500 K at pressures up to 35 MPa, and yield absolute results in fully automated operation. Temperature measurements are accurate to 10 mK and pressure measurements are accurate to 0.002 MPa. The isochoric method utilizes pressure *versus* temperature measurements along an isomole and detects phase boundaries by locating the change in the slope of the isochores.

The experimental data from four gas samples show that cubic equations of state, such as Peng-Robinson and Soave-Redich-Kwong have 1-20% errors in predicting hydrocarbon mixture dew points. The data also show that the AGA 8-DC92 equation of state has errors as large as 0.6% when predicting hydrocarbon mixture densities when its normal composition range is extrapolated.

ACKNOWLEDGMENTS

I would like to express my sincere gratitude to my committee chair and research advisor, Drs. K. R. Hall and J. C. Holste, for their continual interest, guidance, and support throughout the course of this research. Their expertise in thermodynamics improved my research skills and prepared me for future challenges. I thank my other committee members Dr. Philip T. Eubank and Dr. Donald G. Naugle for their time and valuable comments during this work.

I would like to thank all the graduate students in the thermodynamic research group for their help and advice.

I would like to thank Mr. Randy Marek for his valuable advice in every step of the construction of the apparatus. I also would like to thank him for his kindness and friendliness.

Finally, I thank my family: my wife, Hong Du, for giving me the most patient and loving support and encouragement to my work, and her many good suggestions to my dissertation; My parents, for their ever-loving support and understanding during the years of my studies and work in U.S.A.

While all of the people mentioned here have contributed to the dissertation in one way or another, directly or indirectly, and share the credit of the better parts, only I am responsible for any inconsistencies, errors and other shortcomings it may still contain.

TABLE OF CONTENTS

TABLE OF CONTENTS (Continued)

Page

TABLE OF CONTENTS (Continued)

Page

LIST OF FIGURES

FIGURE Page

LIST OF FIGURES (Continued)

FIGURE Page

LIST OF TABLES

INTRODUCTION

Natural gas is among the cleanest, safest, and most useful of all energy sources. It is used extensively in residential, commercial and industrial applications, and it is the most common energy source used for home heating with about 55 percent of American homes using gas. In 1998, there were more than 1 million new residential natural gas customers, increasing the nationwide total to about 56 million homes. The use of natural gas is also rapidly increasing in electric power generation and cooling, and as a transportation fuel.

According to Gas Research Institute (1999), primary gas demand in 1997 was 22.4 quadrillion Btu, and that demand should increase almost 44% by the year 2015. Along with that, primary gas consumption is projected to increase about 2% per year, which represents a rate about two-thirds faster than the rate of growth in total primary energy consumption (Table 1). Because of this, GRI projects that the gas will capture a growing share of total primary energy consumption, increasing from 24% in 1997, to 28% in 2015. Clearly, the need for research to improve engineering methods applied in utilizing this resource is self evident because of its impact throughout our society.

To achieve this kind of impressive growth, a number of things must fall into place. The world must increase exploration and production for its natural gas resources. The existing natural gas transmission and distribution infrastructure must be expanded.

This dissertation follows the style of *AIChE Journal*.

Advances in technology, from production to gas-to-liquid technologies must continue. In addition, and the main topic in this dissertation, the natural gas thermodynamic properties must be known accurately for many important operations of the natural gas industry. Of the thermodynamic properties of the natural gas mixtures that are of significance, the density is of special importance because a huge amount of natural gas undergoes custody transfer each day. During exploitation of a gas reservoir, the phase behavior of the fluid becomes important in certain stages of the process and it certainly of vital importance during refining and transportation.

Table 1. Primary Energy Consumption (Quads)

	1997	2000	2005	2010	2015
Petroleum	36.4	36.9	39.6	42.0	43.7
Gas	22.4	23.6	25.9	28.9	32.1
Coal	21.3	21.9	23.9	24.9	27.0
Nuclear	6.7	7.2	6.7	6.6	4.8
Hydro	3.5	3.1	3.1	3.2	3.2
Other	3.5	3.8	4.1	4.7	5.0
Total	93.8	96.5	103.3	110.3	115.8

Natural Gas Density

Accurate flow metering at high pressure is required for the sale and purchase of natural gas by volume. Such so-called ‘custody transfer’ sales may be between companies within or across national boundaries and be controlled by either national measurement standards or contracts based upon international standards produced by committees of organizations such as: International Standards Organization. Corrections

to measured volumetric flow rates in term of the non-ideal behavior of natural gas at high pressure are necessary. These usually take the form of compressibility factor corrections. It is interesting that although the most popular flow metering method, the orifice plate, has only a moderate accuracy, international standards (hence purchase contracts) require relatively high accuracy in compressibility factors used (Starling et al., 1986). The equation of state most widely used for calculating natural gas density (compressibility) is the Detailed Characterization Method or AGA8-DC92 (Starling and Savidge, 1992) equation developed by the American Gas Association. This equation is valid for lean natural gas mixtures over a wide range of conditions, but its application to rich natural gases (those containing heavier hydrocarbons), as encountered in gas condensate fields in Deepwater Gulf of Mexico, is untested. This model must be validated with reliable data obtained on a limited number of samples that have well defined compositions. Although, several studies have provided experimental data for mixtures containing natural gas constituents, accurate density data are not available in certain ranges of temperature, pressure and composition. In our group, we perform highly accurate density measurements using an isochoric apparatus combined with a magnetic suspension densimeter.

Hydrocarbon Dew Point

Hydrocarbon dew points in natural gas mixture are important quality parameters stipulated in contractual specifications and enforced throughout the supply chain, from producers to transmission and distribution companies and final end users. Accurately

monitoring hydrocarbon dew point temperature in natural gas is therefore vital if the integrity and quality of the gas are to be reliable and contractual agreements satisfied (Benton, 2002).

Hydrocarbon dew point is the temperature at which hydrocarbon condenses first forming when natural gas cools, at constant pressure, and thus ceases to be wholly gaseous. In many cases, however, avoiding the formation of such liquids in natural gas is of critical importance. In order to avoid two-phase flow in such systems, which might well make compressors designed for gas transport inoperable, a common practice is to operate the gas-gathering operation in the so-called dense phase region, which is the region at pressures above the maximum in the two-phase envelope where the mixture is always single-phase. Clearly, it would be wasteful in compression costs to operate at higher pressures than absolutely necessary, and operation as close as possible to the cricondenbar of the two-phase envelope is necessary (Melvin, 1988).

Dew points of natural gas mixtures are highly sensitive to the small fractions of higher alkanes in the fluid, and prediction of the dew point curve with current equations of state (EOS) is unreliable (May et al., 2001). Given the economic value of phase behavior information, experimental measurement is the only sufficiently accurate means of determining the dew point curve at the present time.

The isochoric technique is used in this research. This technique is an attractive method for carrying out precise *pVT* and phase equilibrium measurements. One of the features is its amenability to automation, thus moderating the effort level usually

associated with experimental work in this field. Furthermore, the method yields densities, in the homogeneous fluid regions, and the location of phase boundaries.

Objectives

The following tasks compose this research project:

1. Design and construct the new apparatus. The apparatus has been designed and constructed to comply with the following requirements:
   - It should be automated.
   - The pressure and temperature ranges should be up to 35 MPa and 200 K to 500 K respectively.
   - The pressure and temperature measurements should be precise and accurate.
   - It should be possible to make measurements over a wide range of states from a single loading.
   - Easy access to any parts of apparatus is desirable for maintenance.
2. Test the apparatus performance by measuring pure propane and carbon dioxide vapor pressures.
3. Collect *pVT* data and determine the dew point of four natural gas mixtures of commercial interest. The compositions of the mixtures (mol% methane: 91%, 94%, 88%, 78%) are representative of those encountered in gas industry operations in deepwater of Gulf of Mexico. DCG Partnership Inc and Accurate Gas Product Inc. prepared the mixture samples. .

4. The experimental densities and phase loops will be compared to simulation data predicted by several commercial software.

It is expected that this research will provide essential densities and phase envelope data for designing natural gas pipeline systems and validating new equations of state for natural gas mixtures.

LITERATURE REVIEW

In this chapter, several experimental methods for high-pressure vapor liquid equilibrium and high-pressure density measurement are reviewed. The relative strengths and weakness of each method are discussed. Finally, we discuss the philosophy of our experimental approach to *pVT* studies.

High Pressure Vapor-Liquid Equilibrium Measurement

High-pressure vapor-liquid equilibrium (VLE) can be classified as either analytical or synthetic (Deters and Schneider, 1986). In the analytic method, temperature or pressure is adjusted to bring about phase separation. Samples are then withdrawn from the phases and analyzed by gas or liquid chromatography. This technique may be subdivided into static, dynamic and circulation methods. The experimental results from this type of experimental equipment are usually isothermal or isobaric phase diagrams. For this work, natural gas mixtures are of concern, which often contain a small fraction of heavy components (C_{7+}), which are difficult to measure accurately, especially in phase equilibrium studies. So, in this review, we focus upon the synthetic method. In the synthetic method a mixture of known composition is prepared and its behavior observed as a function of pressure or temperature. The experimental results from this type of equipment are isopleth phase diagrams. The synthetic method may be subdivided into visual and non-visual.

Visual Methods

In the oil and gas industry, the use of manually operated ‘cooled’ or ‘chilled’ mirror dew point meters is the simplest and most widely applied method of hydrocarbon dew point measurement. These instruments have a metallic mirror surface inside a high-pressure sample cell. The instruments are also equipped with a glass viewing port through which operator can observe the mirror surface. Mirror dew point meters normally are used for periodic spot check measurements (Benton, 2002).

The principle of the mirror dew point meter is to observe the very first signs of condensate. The main difficulties in making such a measurement lie in the characteristics of hydrocarbon condensates. The natural gas condensates are colorless and have low surface tension. This means that the liquid film that forms as the sample cools through the dew point temperature is almost invisible to operators. At the same time, the decreasing temperature measurement reading must be observed as the mirror temperature drops. To achieve the best sensitivity and repeatability of measurement, the rate of mirror cooling is critical and should be as slow as possible through the region in which the dew point is likely to be found (Warner et al., 2001). The subjective nature of such a measurement technique can result in large uncertainty in natural gas dew point measurement (Benton, 2002).

Non-Visual Methods

The method usually involves a blind *pVT* cell filled in the single-phase region with a mixture of known composition. Variation of one of the measured quantities allows measurement of a second quantity while the third is held constant. That is,

measurements are made along either an isobaric or isochoric or isothermal path with the homogenous /heterogeneous boundary determine from a discontinuity in the slope of the other two variables (Eubank et al., 1980). We discuss the isochoric technique in detail.

High Pressure Density Measurements

Magnetic Suspension Densitometer

In the early 1980s, Kleinrahm and Wagner (1986) developed a high-accuracy densitometer. The method used for the density measurement is based upon the Archimedes buoyancy principle. The principle states that the upward buoyant force exerted on a body immersed in a fluid is exactly equal to the weight of the displaced fluid. Thus, the density of a sample in the measuring cell is:

$$\rho = \frac{m_s - m_s^*}{V_s} \tag{1}$$

where m_s is the 'true' mass of the sinker, m_s^* is the 'apparent' mass of the sinker, surrounded by the sample fluid, and V_s is sinker volume.

Two sinkers densitometers compensate for all side effects (such as zero-point shift of the balance, adsorption effects.) which reduce the accuracy of the density measurements. A critical component of this technique is the magnetic suspension coupling. The suspension force is transmitted from the high-pressure densimeter to the analytical balance at ambient temperature and pressure through this coupling without physical contact. The coupling consists of a permanent magnet connected by a thin wire to the sinker support, an electro-magnet attached to the weighting hook on the underside

of the balance, and a position sensor and a control system. The pressure-proof coupling housing is made of beryllium copper, a magnetically neutral metal. In the present state, the two-sinker densitometer covers a temperature range form 60 to 340 K, a pressure range from 0.001 to 12 MPa, and a density range from 1 to 2000 $kg.m^{-3}$. The total uncertainty is $< \left|1.0 \cdot 10^{-4} \cdot \rho\right|$ to $< \left|1.5 \cdot 10^{-4} \cdot \rho\right|$ in nearly the entire measuring range.

In order to extend the instrument measuring range towards higher temperatures and pressures, Wagner et al. (1995) have developed a new type of "single-sinker densimeter". Although the single sinker basic design is much simpler than that of the two-sinker densimeter, it is also possible to perform highly accurate density measurements at relatively low gas densities by applying some of the advantageous features of the two sinker principle (Goodwin et al., 2003). At present, a compact version of the single-sinker densimeter has been built and used in Texas A&M University. This densimeter is specially designed for pressures up to 200 MPa and temperatures from 200 to 530 K. The uncertainty in density is around $\pm$ 0.05 per cent.

Vibrating Tube Densimeter

In the vibrating-tube technique, the density is determined from the resonant frequency of a U-shaped tube. Oscillations are close to the resonant frequency of the tube and are related to the mass of the tube and density of fluid inside the tube. A vibrating tube is fundamentally similar to a vibrating rod clamped at both ends and the same formalism is used for describing the oscillations. The following empirical equation is used to calculate the fluid density (Goodwin et al., 2003):

$$\rho = K \tau^2 + L \qquad (2)$$

where τ is the period of vibrator, and ρ is the density of fluid contained in the tube. K and L are instrument calibration constants that can be deduced from measurements on the two fluids having well-known properties (such as water and iso-octane).

The vibrating tube densimeter is not an ideal linear oscillator because the resonant frequency depends upon amplitude. There is also the phenomenon of creep which means that the elastic constants of the vibrating tube shift with age and use, and especially from shocks. These non-ideal behaviors of vibrating-tubes require vibrating-tube densimeter to be calibrated very carefully and frequently to maintain the expected accuracy. Bouchot et al. (2001) and Goodwin et al. (2003) review the application of vibrating tube densimeter in thermodynamic properties measurement.

Burnett Methods

Burnett (1936) determined the densities of sample fluids without measuring the mass or volume directly. Only pressure and temperature are measured before and after expansion of the sample from a single volume (V_A) into the combination of the original volume and a second volume ($V_A + V_B$). The densities of the fluid at these two instances are related to the volumes of the two chambers as

$$\frac{\rho_{i-1}}{\rho_i} = \frac{(V_A + V_B)_i}{(V_A)_{i-1}} = N_i \tag{3}$$

therefore

$$\rho_i = \rho_m \prod_{j=i+1}^{m} N_\infty \left[\frac{1+\gamma_{AB} P_j}{1+\gamma_A P_{j-1}} \right] = \rho_m N_\infty^{m-i} \prod_{j=i+1}^{m} \left[\frac{1+\gamma_{AB} P_j}{1+\gamma_A P_{j-1}} \right] \tag{4}$$

where γ is the pressure distortion coefficient for a given temperature, and N_∞ is the cell constant at zero pressure. The data are analyzed using a virial equation of state in the region that is applicable. Combining the density virial equation

$$P_i = RT\sum_{k=1}^{M} B_k \rho_i^k \tag{5}$$

with equation (4), yields

$$P_i = RT\sum_{k=1}^{n} B_k \left\{ \rho_m N_\infty^{m-i} \prod_{l=i+1}^{m} \left[\frac{1+\gamma_{AB} P_l}{1+\lambda_A P_{l-1}} \right] \right\}^k \tag{6}$$

where n is the estimated optimum number of virial coefficients, B_k are virial coefficients and i stands for the i-th stage. The fitting parameters N_∞, B_k and ρ_m can be obtained using a special data reduction technique (Stouffer et al., 2001). The error in the cell constant is compounded into the density value.

The Burnett technique may be coupled with isochoric techniques to provide more efficient measurements. The Burnett experiment does not lend itself easily to automation because of the required opening and closing of valves; also, because of innate accumulation of error, the very high precision required in the pressure measurements necessitates the use of high-quality dead-weight gauges that usually are operated manually. By combining Burnett expansions along one isotherm with isochoric measurements at other temperatures, the measurement can be partly automated with only little loss in accuracy (Linsky et al., 1987). Straty and Palavra (1984) determined the isothermal density for propane at the reference temperature 523.15 K using an apparatus based upon the Burnett method. They coupled this apparatus to an isochoric one which

in turn provided the density of the fluid at higher temperatures. Densities were determined from the intersection of the pseudo-isochores with the isotherm previously obtained by the Burnett method.

Burnett method and its variations continue to be appropriate techniques for determination of densities. In general, however, Burnett methods are labor intensive and involve complex measurement procedures compared to the other techniques (Goodwin et al., 2003).

Isochoric Methods

The isochoric technique is another attractive method for performing precise PVT and phase equilibrium measurements, and it has been used by several investigators, including: Goodwin (1961), Eubank (1980, 1987), Straty and Palavra (1984), Yurttas (1994), Duarte-Garza et al. (1995), Nicola et al. (1998), Fenghour et al. (1999). One of its features is its amenability to automation thus moderating the effort level usually associated with experiment work in this field. In the isochoric method, the temperature is changed by a selected increment, a new equilibrium (p, T) point is then determined. This process is repeated until the preset pressure or temperature is reached.

Phase changes are accompanied by a discontinuous change in the slope of an isochore. As shown in Figure 1, an isochore is a constant density path on a phase diagram. By plotting many isochors the complete phase boundary of a given system can be determined.

Isochoric *pVT* data, obtained with extremely high precision, give valuable information on the thermodynamic properties of dense fluids. The isochoric technique

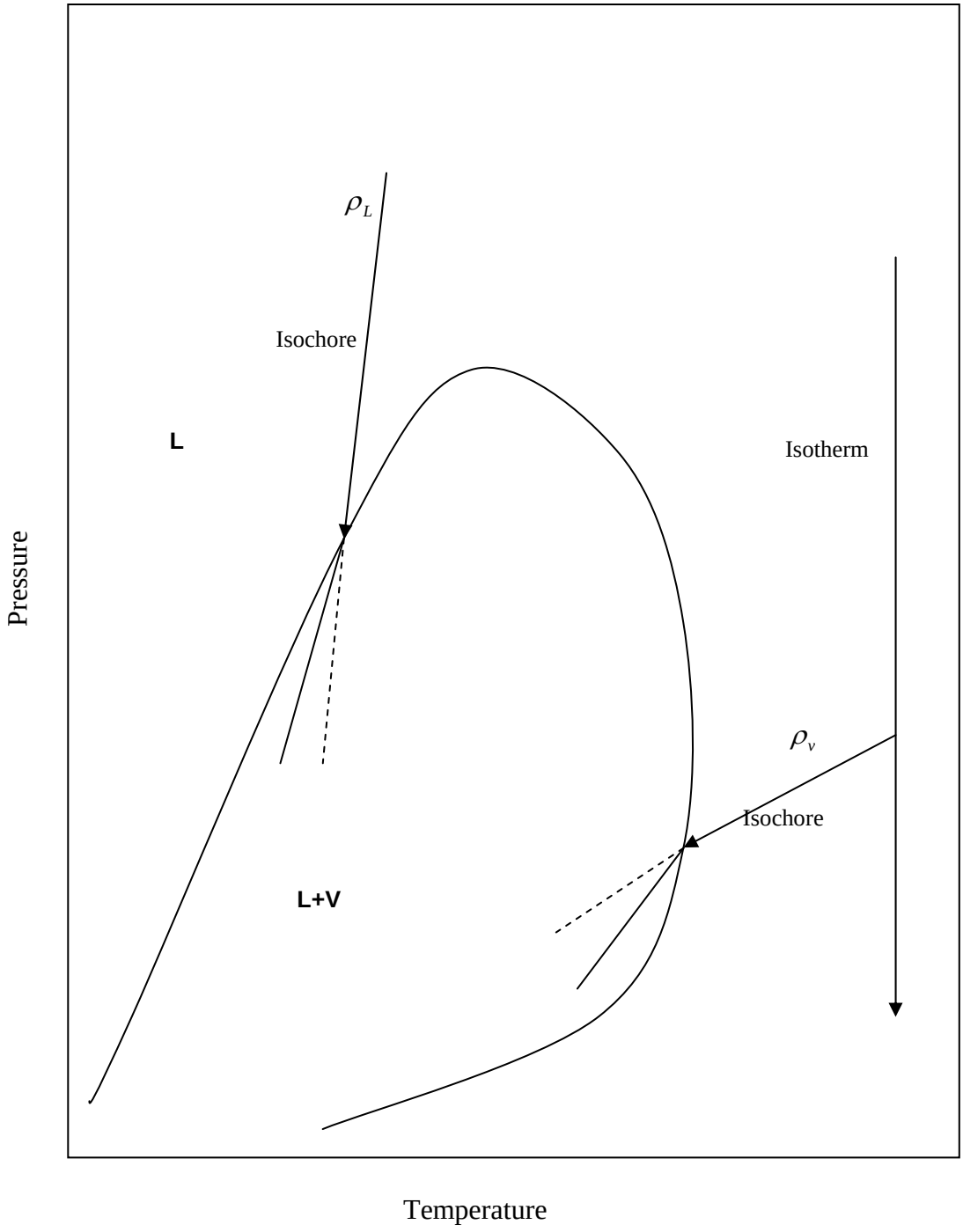

Figure 1. Phase diagram for a mixture.

measures $(\frac{\partial P}{\partial T})_V$ and $(\frac{\partial^2 P}{\partial T^2})_V$ which are needed to calculate thermodynamic functions. For example, enthalpy changes can be derived from isochoric *P-V-T* measurements by making use of several thermodynamic relations (Stouffer et al., 2001):

$$\Delta U = \int \left[T\left(\frac{\partial P}{\partial T} \right]_V - P \right] dV \tag{7}$$

The quantity $(\frac{\partial P}{\partial T})_V$ is the change in pressure with respect to temperature at constant volume, which is also the slope of an isochore. Therefore, by determining the slope of experimentally determined isochores, changes in internal energy, ΔU, may be derived. This equation shows the strength of the isochoric apparatus. An isochoric apparatus measures isochoric slopes almost directly, while other apparatus require more calculations, and therefore introduce more uncertainty into the calculation of changes in internal energy. The details of calculating other energy function (enthalpies, Helmholtz free energies, Gibbs free energies, entropies) appear in Kellerman (1994).

Lines of constant density or isochores, which show simpler behavior than isotherms and isobars have been observed to be nearly linear with temperature (Frederick et al., 1919). Curvature of the isochore determines the change of the specific heat C_v, with density at constant temperature (Diller, 1971); that is

$$\left(\frac{\partial^2 P}{\partial T^2} \right)_\rho = -\frac{\rho^2}{T} \left(\frac{\partial C_v}{\partial \rho} \right)_T \tag{8}$$

therefore, deviations from linearity are important and have significant physical implication.

An isochoric method was selected for this work because it is a convenient method from an experimental point of view. At Texas A&M other devices including a magnetic densimeter and a Burnett apparatus are used in addition to the isochoric apparatus to capitalize on the strengths of each device and to cross-check data.

In the past, *pVT* data were collected at Texas A&M using a semi-automated isochoric apparatus in addition to several other devices. This device was constructed and operated as part of the dissertation work of Yurttas et al. (1994). The original goal was for the device to be fully automated, however this proved difficult, and a semi-automated design was implemented. An alternative design was proposed and some early feasibility calculations performed by Matabe (1999) indicated that the device could be redesigned in such a way that it could be fully automated without an appreciable effect on the accuracy of the instrument. This research provides detail of the design of a new apparatus for natural gas mixtures.

Data Analysis in Isochoric Method

Analysis of the isochoric data consists of two major elements: (1), location of the phase boundary and (2), calculation of the gas density from isothermal (Magnetic Suspension Densimeter) measurements.

The slope $(\partial P/\partial T)_\rho$ of an isochore change discontinuously at the two-phase boundary, as shown in Figure 1. This change of slope is used in this work to locate the two-phase envelope. The isomoles are corrected to isochores and a polynomial of the form,

$$P = \sum_{i=1}^{n} a_i T^{i-1} \tag{9}$$

is fit to the isochores.

For each isochore, equation (9) is fit repeatedly, adding one measurement at a time from higher to lower temperature. The deviations increase abruptly when the first measurement from the two-phase region is added. The deviations of all two-phase region measurements are fit using a second polynomial

$$P_{exp} - P_{cal} = \sum_{i=1}^{n} a_i T^{i-1} \tag{10}$$

Here P_{cal} is the pressure calculated from the single phase fit. Solving equation (10) for zero yields the temperature at the intersection between the single and two phase polynomials. Inserting the phase boundary temperature into equation (9) yields the corresponding pressures.

We should point out that the discontinuous change in the slope of an isochore is difficult to detect near the cricondentherm (local maximum on temperature in a P_T diagram). Furthermore, it can be proved that for mixtures (Eubank et al., 1987), the slope of an isochore is continuous at the cricondentherm.

The base densities for each isochore were determined from the isothermal densities. The isothermal densities were measured with a magnetic suspension densimeter which had a claimed uncertainty of 0.1%. These densities results were used to determine the parameters a_i in

$$P = \sum a_i \rho^i \tag{11}$$

for each isotherm.

Because the volume of the isochoric cell changes with variations in temperature and pressure, the density of a constant mass sample is not constant. The actual densities are calculated using the volume change of the cell as a function of temperature and pressure:

$$\frac{V(T,P)}{V_0(T_0,P_0)} = 1 + \gamma(P - P_0) + \beta(T - T_0) \tag{12}$$

where $\gamma = 2.53 \times 10^{-5}\,\mathrm{MPa}^{-1}$ and $\beta = 4.86 \times 10^{-5}\,\mathrm{K}^{-1}$. The pressure coefficient γ is the inverse of the bulk modulus of the cell material. It may also be approximated from equations describing the change in cell geometry (Stouffer et al., 2001).

In order to estimate the precision of equation of state results, we compare equation of state predictions to the experimental data. We have chosen three equations of state: the Peng-Robinson (Peng et al., 1976), Soave-Redlich-Kwong (Soave et al., 1979) and AGA8-DC92 for comparison of gas mixtures and Wagner equations for comparison to pure components.

APPARATUS

In this section we present a detailed description of the new isochoric apparatus. The apparatus operates at temperatures ranging from 200 K to 500 K and at pressures up to 35 MPa. Figure 2 shows the overall arrangement of the isochoric apparatus. Essentially, it is: an isochoric cell with a vacuum chamber and an isothermal shield, an automated pressure measurement system, an automated temperature control and measurement system, a high pressure gas manifold system, and a high vacuum system.

Isochoric Cell

Our design objectives were (1) to change temperature and establish temperature equilibrium very rapidly, (2) to control temperature to 0.005 K (5 mK) or better, (3) to minimize temperature gradients at equilibrium at less than 0.005 K. A detailed design of the isochoric cell appears in Figure 3.

Ideally, the isochoric cell volume should remain constant for different experiment condition to ensure the experiment is truly isochoric. In reality, all materials of construction are subject to changes in volume caused by changes in temperature and pressure (especially temperature). Materials with low coefficients of thermal expansion are desirable for sample cell construction. Additionally, the sample cell must contain fluids over a wide range of temperatures and pressures (200 to 500 K and up to 35 MPa for this apparatus), requiring a material with high tensile strength. Also the cell must have a high thermal conductivity and low heat capacity, so the temperature of the cell can change quickly from one temperature set point to another. A high strength to weight

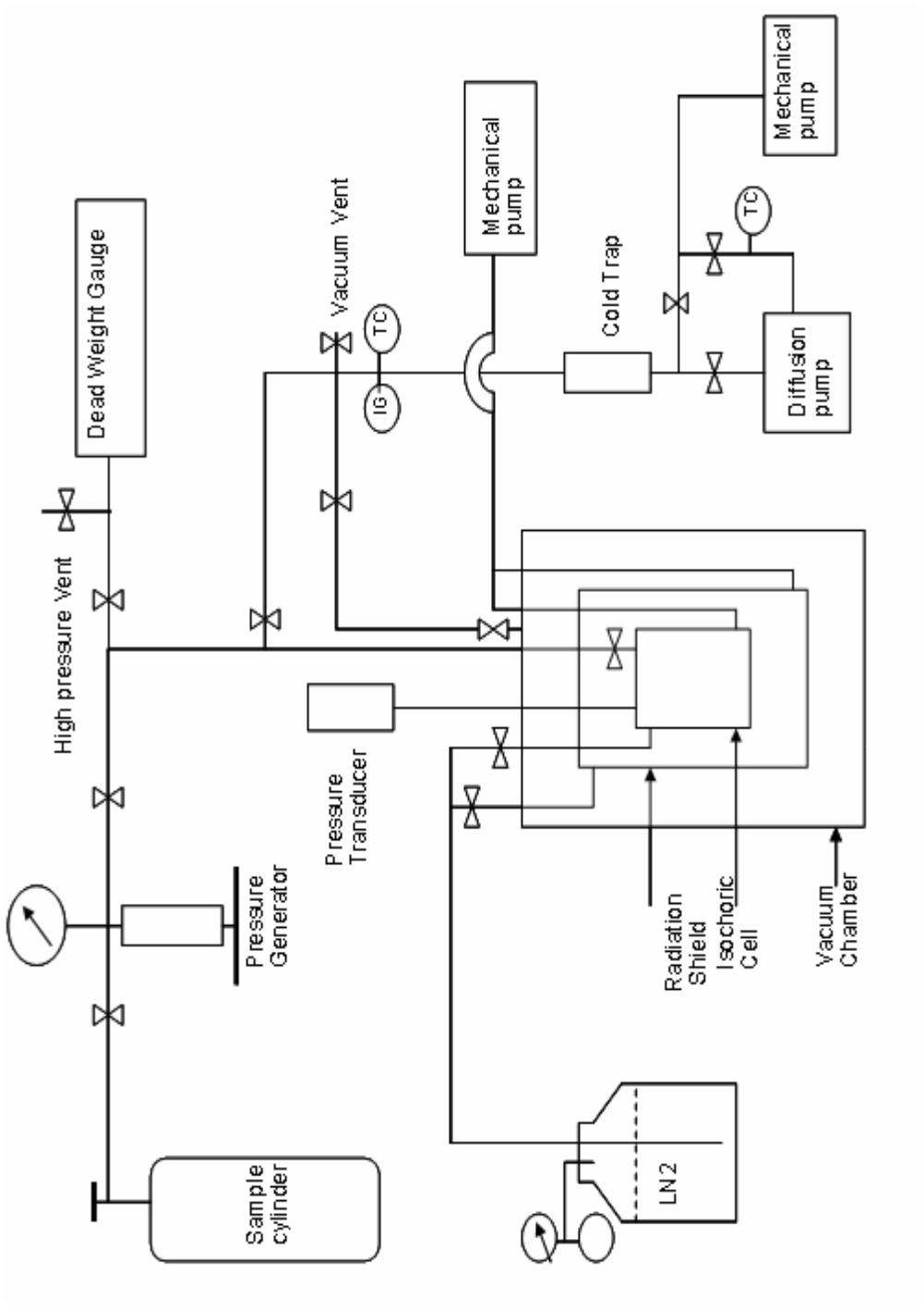

Figure 2. The schematic diagram of isochoric experiment.

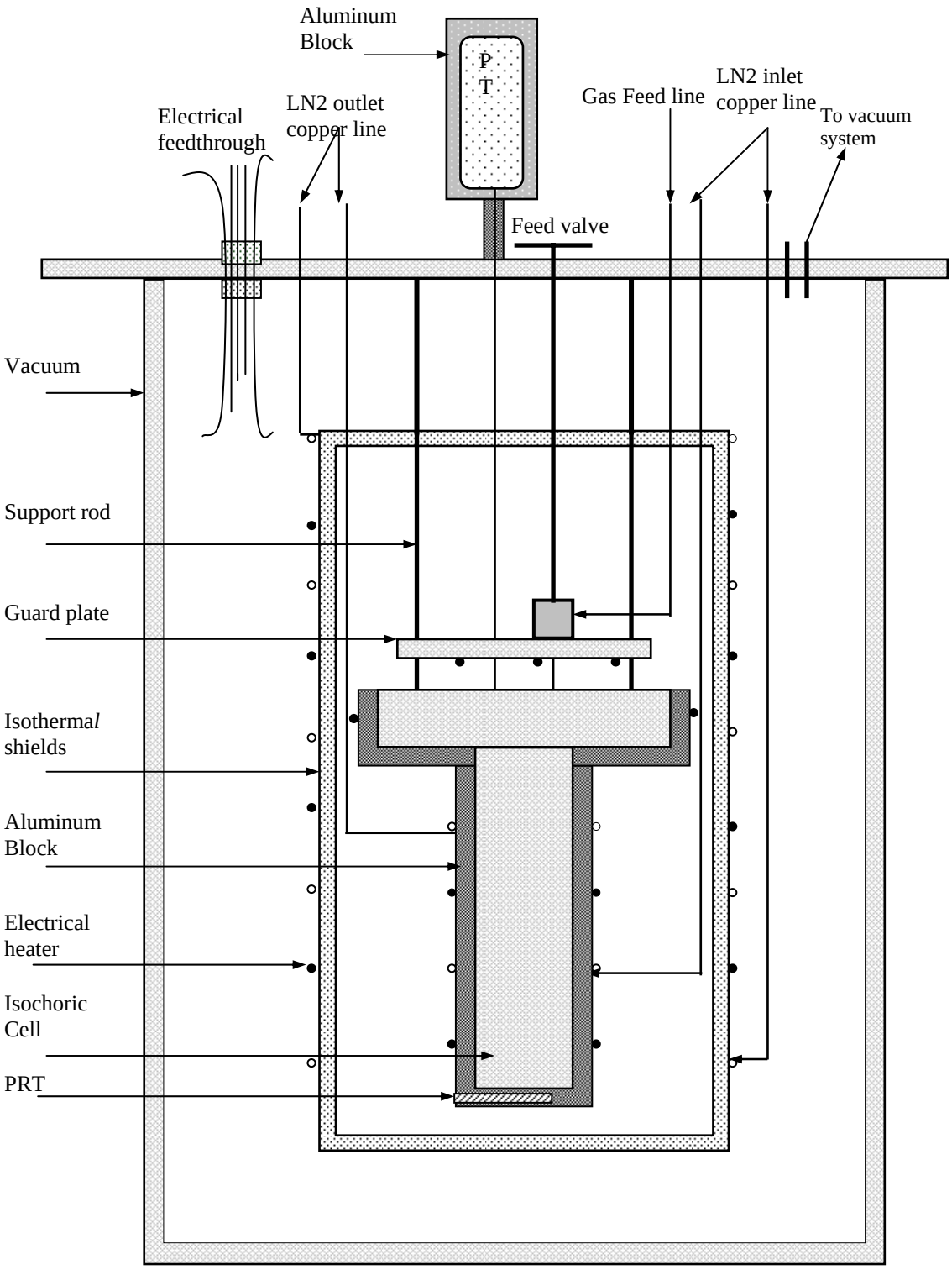

Figure 3. Isochoric cell.

ration is useful for better and faster temperature control, because the thermal mass of the cell can be minimized by reducing the total mass of the cell.

Some natural gas mixtures may contain hydrogen sulfide, H_2S, which corrodes many metals, so the cell must be chemically inert. Otherwise, the sample composition can change from chemical reaction of cell with the sample, and the mechanical integrity of the cell may be destroyed. Type 316 stainless steel is an ideal construction material for this apparatus, however the stainless steel thermal conductivity (0.3 J/(s. cm. K)) is lower compared to metals like aluminum (3.0 J/(s. cm. K)) and copper (7.1 J/(s. cm. K)). This low thermal conductivity makes it more difficult to achieve uniform temperature across the isochoric cell; however stainless steel is the best choice for satisfying the above criteria.

It is important to reduce the mass of the isochoric cell in addition to restricting cell volume changes. We accomplish this by reducing the openings and connections to isochoric cell. The cell has only two openings (connections to the transducer and the feed valve) and one seal. Previous apparatus have contained delta-ring seals and c-ring seals to insure the isochoric cell is leak-proof (Lau, 1986; Duarte-Garza et al., 1995). The current isochoric cell design employs a seal manufactured by Garlock Helicoflex, a subsidiary of B. F. Goodrich. The Helicoflex seal is a reverse C-ring (Figure 4) that contains a spring specifically chosen for the operating conditions.

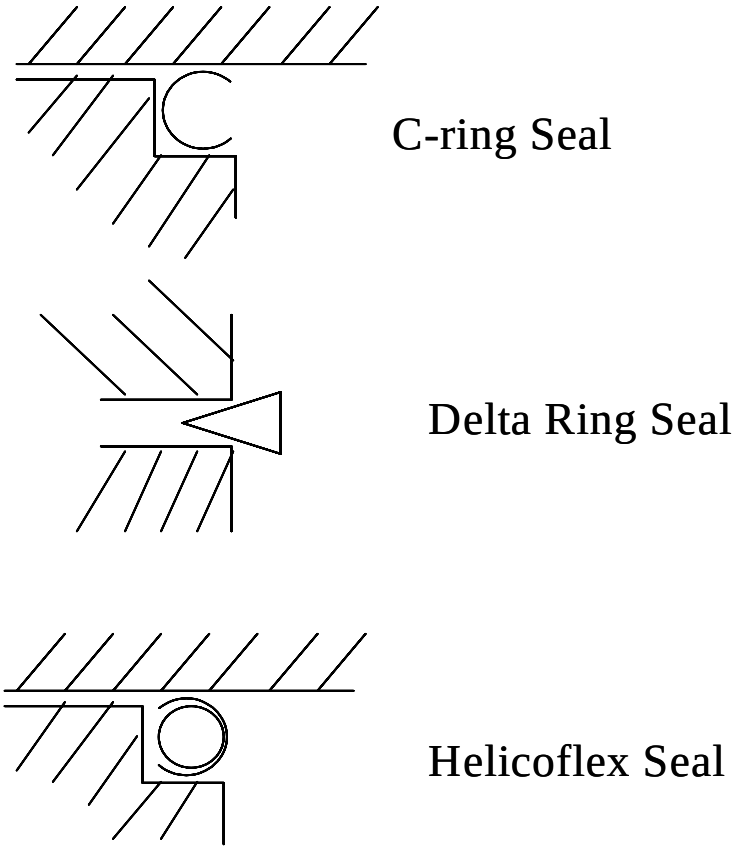

Figure 4. Ring cell cross sections.

The isochoric cell can operate from 200 K to 500 K and full vacuum to 35 MPa. The cell has a cylindrical shape for ease of construction. The thermal conductivity of the stainless steel cell is higher than the thermal conductivity of the natural gas sample, so decreasing the average distance between a sample molecule and the cell wall causes heat transfer to occur more rapidly. Furthermore, a cylinder requires only a small seal. A sphere would reduce the volume of metal necessary to contain the fluid; however it would require a large seal along a great circle of the sphere as a construction limitation. The inner surfaces of the cell are polished to minimize adsorption effects. The isochoric

cell has been tested successfully up to a pressure of 10,000 psia at room temperature. The details of the isochoric cell design are available in the undergraduate thesis of Johansen (2001).

High Pressure Gas Manifold System

The high pressure gas manifold system consists of a variable volume cell (hand pump), a high pressure gauge, and a set of high pressure valves. The feed manifold connects the cell to a high-pressure dead weight gauge (DH instrument, model 26000), the vacuum system, the sample cylinder and the vent line. The sample cylinder is enclosed in a pressure-proof oven and the oven temperature is maintained at well above the natural gas sample cricondentherm.

A commercial nonrotating-stem valve (316 SS) isolates the isochoric cell. The valve features coned and threaded high-pressure connections and Teflon™ packing. The packing is located below the stem threads to prevent contact with media (liquid or gas), and the stem assemblies have non-rotating tips to prevent galling with valve seats. The valve has an extended stem for operation from outside the vacuum can, and the sealing surface is kept small to minimize the torque required for valve closure. The hand pump (Model 37-6-30), which is used to pressurize the fluid into the cell to a desired pressure, has an internal volume of 11 ml, and all the high pressure fittings have cone and thread type of sealing. Stainless steel tubing (1/8” OD) is used for all the high pressure lines. All the components of this manifold are rated to 30,000 psia. The hand pump, valves,

fittings, and tubing are manufactured by HIP (High Pressure Equipment Company, Incorporated).

High Vacuum System

The vacuum chamber isolates the isochoric apparatus and radiation shield from the surrounding environment. The main apparatus is enclosed in this high vacuum system for several reasons. First, the apparatus is designed for operation from 200 to 500 K, so a single liquid bath is not practical for the temperature range desired. Second, by using a vacuum rather than gas environment, little conductive or convective energy transfer occurs at high temperature to the surroundings. Provided there is adequate radiation shielding, no external insulation is required. Third, Oxidation of the internal components at high temperature is greatly reduced in the high vacuum environment. Finally, the apparatus is easier to maintain because only the vacuum chamber and/or isothermal shields need be removed to troubleshoot the internal components and connections of the apparatus.

The vacuum can is bolted to the aluminum support plate and is sealed to the plate with an elastomer O-ring. Each of the feedthrough tubes into the vacuum chamber is sealed at the aluminum support with elastomer O-rings using Cajon Ultra-torr fittings. Likewise, the inlets to the vacuum system are sealed at the aluminum support plate with elastomer o-rings using Key High Vacuum Inc. quick connect fittings.

The whole layout of the high vacuum system appears in Figure 2. The main components of this system are the diffusion pump, the cold trap, the butterfly valves and

the mechanical pump. The system is also equipped with pressure gauges, an ionization gauge and a thermal conductivity (TC) gauge (located at the inlet of the cold trap), and a second TC gauge located in the foreline for control and fault protection. Pressure gauges are controlled by a Varian 843 Rationmatic ionization gauge control.

The ancillary mechanical pump (Welch duo-seal vacuum pump) first brings the pressure inside the vacuum chamber down to about 1 mTorr. At this point, the air-cooled diffusion pump (CVC product type MCF-61C) takes over to create a high vacuum system. Because the diffusion pump cannot exhaust directly to atmospheric pressure, the mechanical pump is used to maintain proper discharge pressure conditions. Unlike mechanical pumps, diffusion pumps have no moving parts and as a result are quite durable and reliable.

One major disadvantage of diffusion pumps is the tendency to backstream oil into the vacuum chamber. The oil can contaminate surfaces inside the chamber or upon contact with hot filaments or electrical discharges may result in carbonaceous or siliceous deposits. For this reason, the systems add a liquid nitrogen cold trap to remove oil particles before they can reach the process stream. The liquid nitrogen is most effective but the most difficult to maintain during continuous operations. The cold trap can last at least 12 hours, and a roughing trap is used to reduce the transfer of mechanical pump oil to the vacuum lines in the event of a power failure. During normal operation the high vacuum system can achieve pressures of 10^{-5} Torr in less than 2 hours.

Data Acquisition and Control

The data acquisition and control system provides automated operation of the isochoric apparatus. Automation frees the operator during data collection, allowing more time for troubleshooting and data analysis. Better measurement precision results from automated data collection by reducing the inherent bias of the operator.

Figure 5 shows the data acquisition scheme for the apparatus. Voltages are measured by a $6\frac{1}{2}$ digit multimeter (Keithley model 2000-20) that communicates with the personal computer through a PCI-GPIB standard interface. In turn, DPDT (double pole and double throw) relays and DC power supplies are controlled with digital and analog signals, respectively. LabVIEW programs provide automated data acquisition and control. LabVIEW controls relay closures, current directions, instrument readings, and heater power. The program employs a proportional and integral (PI) scheme for the apparatus heaters. Other instruments communicate with the computer through RS232. During the heating or cooling stages, monitoring of the temperature and the pressure identifies when the system has attained equilibrium. The computer programs also allow monitoring and complete control to be shifted to any remote location equipped with a modem and a microcomputer.

Temperature Measurement and Control

The logical temperature control algorithm includes temperature measurement, choice of appropriate control action, and conversion of the control action to effect a temperature change. The discussion below describes both the hardware and software needed for temperature measurement and control.

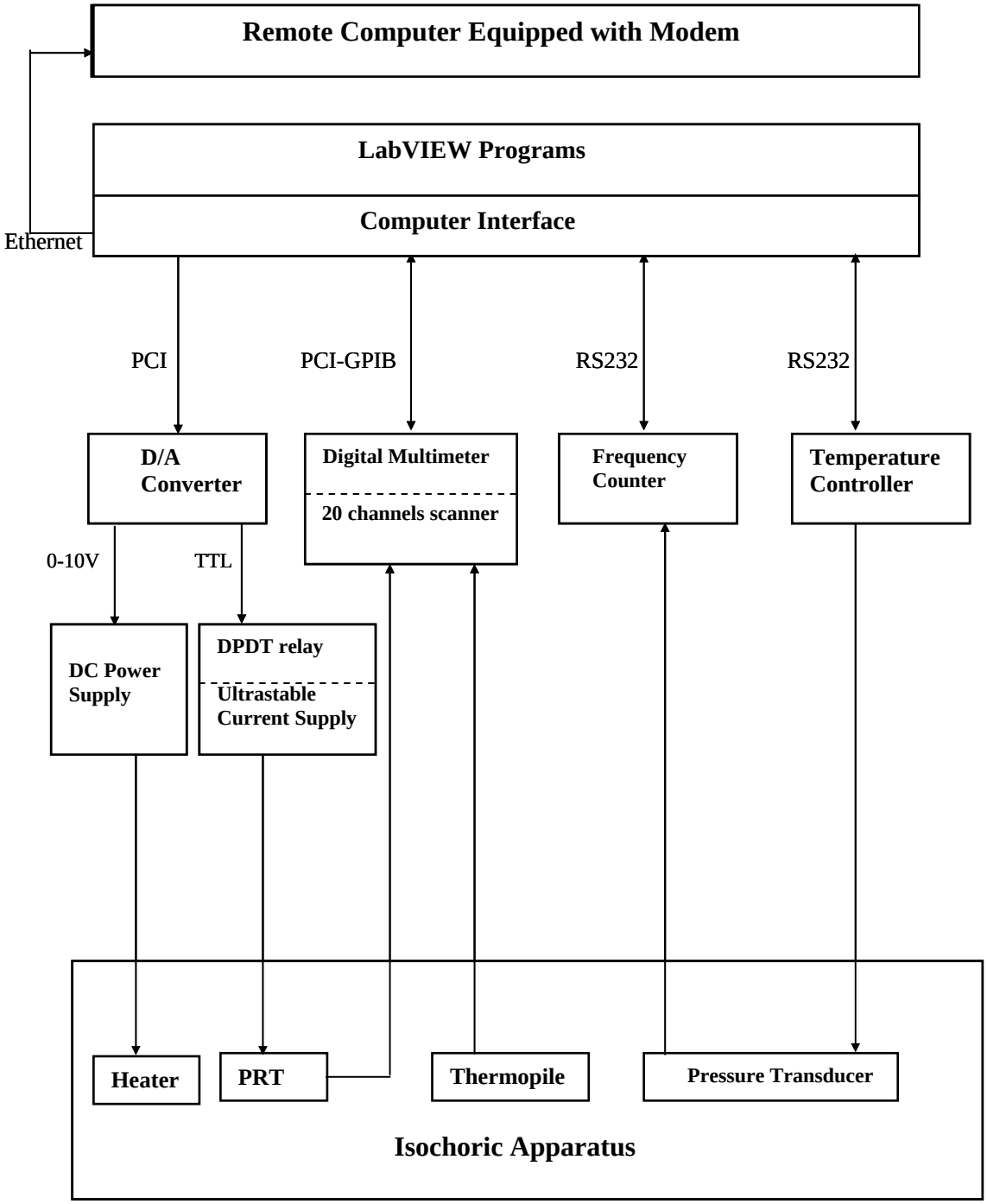

Figure 5. Data acquisition and control.

Temperature Measurement

Temperature can be measured using a diverse array of sensors. Several sensor technologies are available for this purpose, including thermocouples, resistive temperature detectors (RTDs), thermistors, and various semiconductor devices. The measurement range, accuracy, and ease-of-use of these sensors differ considerably, so the selection of a temperature sensor depends upon the specific application. Thermocouples are mechanically simple, durable, and reliable; offer a wide overall temperature measurement range; have accuracies on the order of 1-2 °C. The thermistor (thermally sensitive resistor) is a passive semiconductor device. While thermistors have relatively few drawbacks, it is important to realize that thermistors are relatively low temperature devices, with a typical measurement range of –50 °C to 150 °C. This range is significantly narrower than that of thermocouples and RTD. Platinum resistance thermometers (PRT) are an ideal choice for this project. PRT can measure temperatures over the range 14 K to 500 K to an accuracy approaching 1 mK. They can be cycled repeatedly over several hundred degrees and still provide a very severe test of the best resistance bridges. Few materials can be treated in this manner and remain as stable.

The temperature of the isochoric cell is measured with a four lead platinum resistance thermometer (MINCO Products Inc, Model XS9691). The thermometer was calibrated by Minco Products Inc with respect to IPTS-90. The calibration detail is presented in Appendix A. The PRT were also checked regularly at the tripe point of water, since a change in the triple-point resistance will expose almost all signs of faulty

behavior or misuse. The triple point of water cell was manufactured by Hart Scientific Inc (model 5901).

Resistance thermometers are unlike other temperature sensors in that they require external stimulation in the form of a measuring current or voltage. This gives rise to errors associated with resistance-measuring instruments that must be considered in addition to those caused by the sensor itself.

Figure 6 presents a schematic diagram of the electric circuit used to measure the thermometer resistance. This circuit includes a very stable constant current supply, which provides 0.14 mA to the PRT and a four lead standard resistor (manufactured by Julie Research Laboratories, NY). To achieve high stability, the Zener diode, the operational amplifier, R_{sensor} and R_{ref} all must be stable. The four wires JRL secondary standard resistor, a compact, oil-filled, hermetically-sealed unit, is nominally equal to the ice point resistance of the PRT and is stable with time. The JRL resistor is calibrated by Process Instrument Inc. (Appendix B). The stability for this resistor is 0.003% per year and has 0.02% accuracy. The JRL and PRT are connected in series. The DPDT reed relays have the ability to reverse the current to minimize the effects of thermal EMF using the computer program (the reverse current control signal come from National instrument PCI card that can be programmed to source TTL signal). An external independent DPDT switch provides additional control to reverse the currents.

The voltage on each resistor is measured twice: once with the current in one direction and again with the current in the opposite direction. Subtracting the above two voltage measurements eliminates the offset voltages (including those arising from EMF)

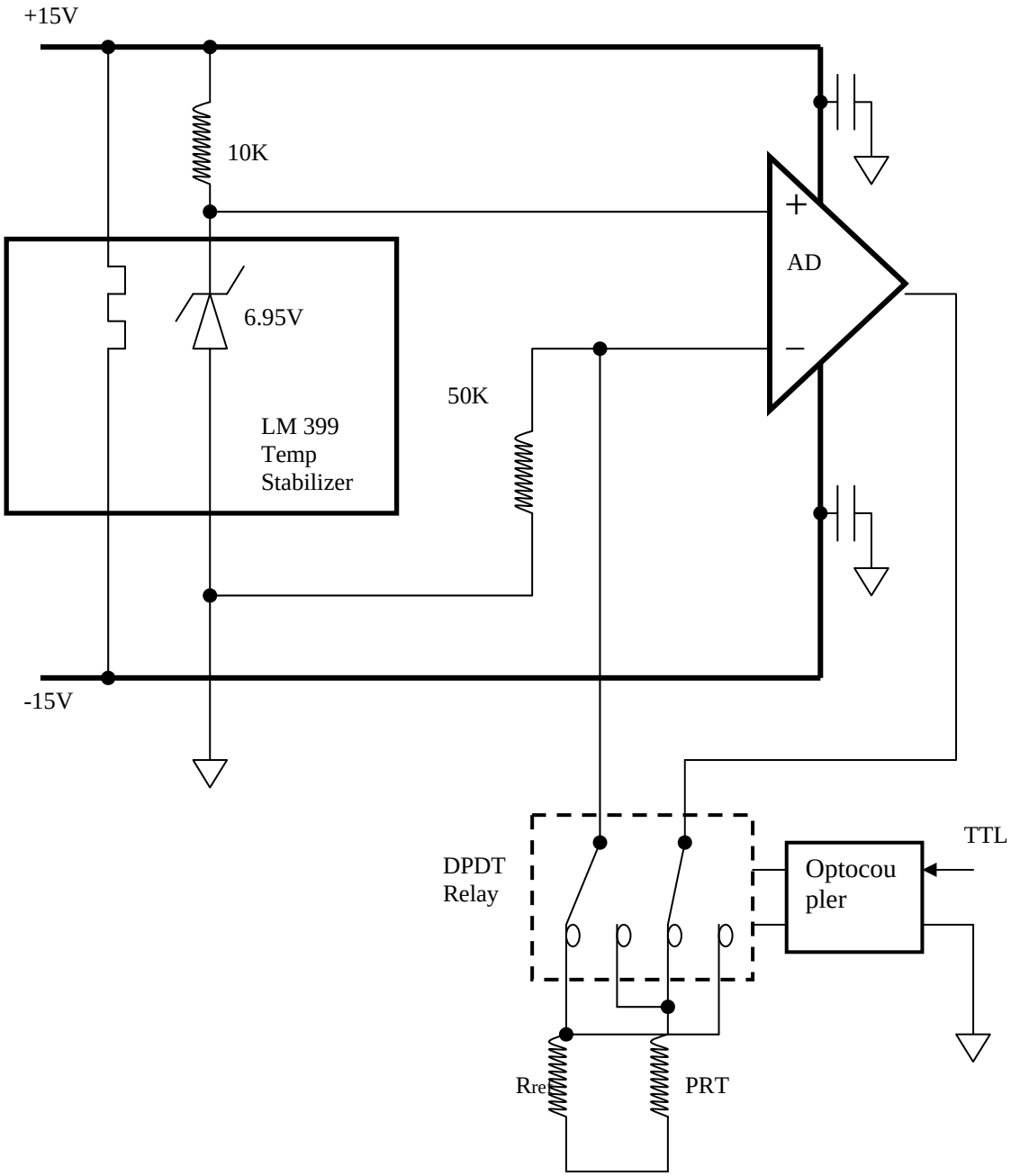

Figure 6. Constant current power supply.

because these offsets are constant. In summary, one ratio measurement requires four voltage samples:

1. PRT, forward current (V_{X1})
2. PRT, reverse current (V_{X2})
3. Reference, forward current (V_{R1})
4. Reference, reverse current (V_{R2})

The voltage samples are subtracted and divided to produce a ratio of sensor resistance to reference resistance:

$$r = \frac{V_{x1} - V_{x2}}{V_{R1} - V_{R2}} = \frac{R_x}{R_R} \tag{13}$$

Using this approach, errors from driving current imprecision, voltage offsets (thermoelectric EMF), and amplifier and ADC inaccuracies are avoided because these all affect the voltage samples equally. Some resistance bridges apply AC driving currents and use sensing circuits that detect only the AC signal, rejecting the DC EMF. The technique is effective at eliminating thermoelectric EMF errors, but it can lead to other errors. Reactance, leakage, and eddy currents become much more significant with AC current.

When a current passes through the sensing element, because of its resistance the element dissipates heat that causes the temperature of the element to increase. This self-heating error can be modeled as the power dissipated divided by the dissipation constant h. Thus the error in the temperature measurement is (Nicholas et al., 1994):

$$\Delta T_m = R(t)I^2 / h \tag{14}$$

where R(t) is the resistance of the sensing element and I is the sensing current. The dissipation constant h is normally expressed in milliwatts per degree Celsius. As we can see from equation (14), the error increases as the square of the current. The current is probably the most significant factor in self-heating. It has been shown (Nicholas et al., 1994) that 1 mA sensing current in a typical application can cause an error as large as 50 mK. To reduce this error, 0.14 mA sensing current is used in the temperature measurement. While lower current is better, currents lower than 0.1 mA result in lower signal levels, which are more difficult to measure.

All other temperatures within the apparatus were measured relative to PRT using two copper-constantan differential thermopiles. The first thermopile measures the temperature gradients between the top and bottom of the cell. The second thermopile measures the temperature gradient between the top of the cell and the guarding plate for isochoric cell. When all of the thermopiles indicate a negligible temperature gradient within the cell (smaller than 0.005 K), then a measurement may be taken and recorded.

A thermopile (TP) is more than one thermocouple (TC) wired in series (Figure 7). The Seebeck coefficient, S, is the response in volts per Kelvins (V/K) a thermocouple has at a given temperature. The Seebeck coefficient for copper-constantan thermocouple fits a quadratic function in temperature (Appendix C). The thermocouple response in the range of 200 to 500 K is 30 to 60 $\mu V/K$. The Keithley DMM2000-20 has 0.1 μV resolutions in voltage measurement, so it can detect as low as 1 mK

temperature difference when five TC's per TP are used in measurement. This sensitivity is better than the goal of temperature control of 5 mK.

$$\Delta T = \frac{\Delta V}{S \times N} \tag{15}$$

where ΔT is the temperature difference, ΔV is voltage signal, N=5;

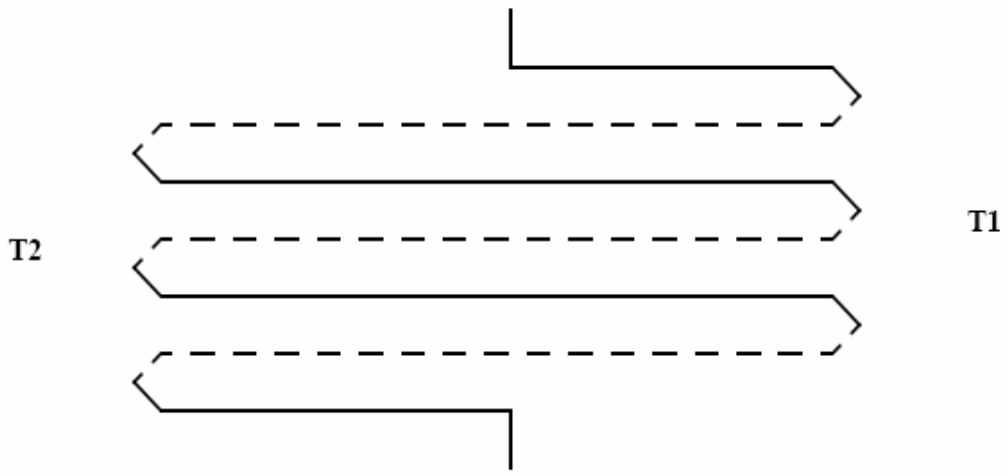

Figure 7. **Thermopile (Solid lines are copper and dashed lines constantan).**

As we can see from equation (15), for a given temperature difference a large signal can be generated that overwhelms any noise from the measurement electronics and switching circuits. Additionally, the selection of type T thermocouples has the advantage that both signal wires are copper, and therefore the thermocouples can be connected to the digital multimeter (DMM) without using an isothermal junction block because the Cu-Cu connection has a much smaller Seebeck coefficient ($<0.2\ \mu V/K$) compared to other metal pairs.

Because a DMM can also measure resistances, it can be used for diagnostic checks of the thermopiles. The resistance of a thermopile is almost constant and stable at a given temperature.

Temperature Control

Heat transfer is accomplished by four main mechanisms: conduction, convection, mass transfer, and radiation. Mass transfer has already been addressed by efforts to insure that the device is truly isochoric. Insulating the sample cell in a high quality vacuum (better than 10^{-4} Torr) nearly eliminates heat transfer by conduction and convection.

Placing an isothermal shield around the cell controls the heat transfer by radiation. The isothermal (radiation) shield consists of cylinder shaped Alumina block controlled at a temperature about 1-5 K below the temperature of the isochoric cell. This temperature is maintained by circulating liquid nitrogen through tubes in the shield or by heating the shield with electrical wires. The isothermal temperature set point is maintained by an Omega temperature controller (model CNi3252-C24) and silicated controller rectifier (SCR) power controller. The SCR is used for isothermal shield heating because of its strong power ability. Because it has limited resolution, the SCR is not used for tight temperature control in the isochoric cell. The heater around the isothermal shield is an Aerobiax mineral insulated, inconel-sheathed heater. The manufacturer ARi industries states that the maximum operating temperature of the heating cable is approximately 1200 K.

Conduction along the feedthroughs and along internal supports from the internal components to the surroundings is minimal. The heat transfer between the cell and the surroundings can take place only by conduction through the supports connecting them. The four supports between radiation shield and the cell are 316 SS rod. Three supports connect the radiation shield to the top plate of the outer vacuum can. Each support consists of 316 SS with numerous offset holes drilled into the outer diameter, giving a honeycomb appearance. Honeycombing minimizes heat conduction along the support by increasing the length of the conduction path.

For operation below room temperature, energy must be removed from the fluid. This is accomplished by cooling the isothermal shield and isochoric cell. The radiation shield cooling coil is composed of 3/16 inch copper tubing anchored to the radiation shield, and the isochoric cell cooling coil is an 1/4 inch copper tubing. The cooling is provided by a low cost system which consists of a 17 Liter liquid nitrogen Dewar and a pressure regulator. The liquid nitrogen leaves the Dewar through 1/4 inch copper tubing. The Welsh Duo-seal vacuum pump is used to drive the liquid nitrogen through the copper tubing, around the isothermal shield and the isochoric cell. After reaching the desired isochoric cell temperature, the liquid nitrogen going to isochoric cell is stopped and the cooling is provided to the isothermal shield only. The liquid nitrogen in the Dewar must to be filled once in every 10 hours. Typically, 0.1 °C temperature stability or better is achieved with the isothermal shields. When the isothermal temperature stability is larger than 0.2 °C, it become very difficult to control the isochoric cell temperature stability to 0.005 K.

The isochoric cell is embedded within a large Aluminum block to dampen temperature gradients within the cell and to aid in bringing the cell to thermal equilibrium faster. We use aluminum because of its high thermal conductivity. Copper has been used in similar applications and, although it has a high thermal conductivity, its density is much higher than that of aluminum.

The temperature of the isochoric apparatus is controlled using a PI (Proportional-Integral) control algorithm. In the PI controller, the set point is compared to the process variable to obtain the error

$$e = SP - PV \tag{16}$$

where SP represents set-point and PV represents process variable. We can then calculate the controller action theoretically as

$$u(t) = K_c \left(e + \frac{1}{T_i} \int_0^t e dt \right) \tag{17}$$

where K_c is controller gain. If the error and the controller output have the same range, that is –100% to 100%, controller gain is the reciprocal of proportional band. T_i is the integral time in minutes (also called reset time). The derivative actions in temperature control are not essential because temperature has a slow response to outside energy change. The PI algorithm is used in a 1 K band around the set point. Outside of the band, the heaters are turned on full power (manually or through computer program) if the temperature is too low or off if the temperature is too high.

The proportional gain and reset time are estimated using an open-loop (step test) tuning procedure. The open-loop tuning procedure assumes that one can model any

process as a first-order lag and a pure dead time. To perform the open-loop tuning procedure, perform the following steps:

1. Put the controller in manual mode, set the output to a nominal operating value, and allow the PV (process variable) to settle completely. Record the PV and output values
2. Make a step change in the output, Record the new output value.
3. Wait for the PV to settle. From the chart, determine the values as derived from the sample displayed in Figure 8.
4. Multiply the measured values by the factors shown in Table 2 and enter the new tuning parameters into the controller.

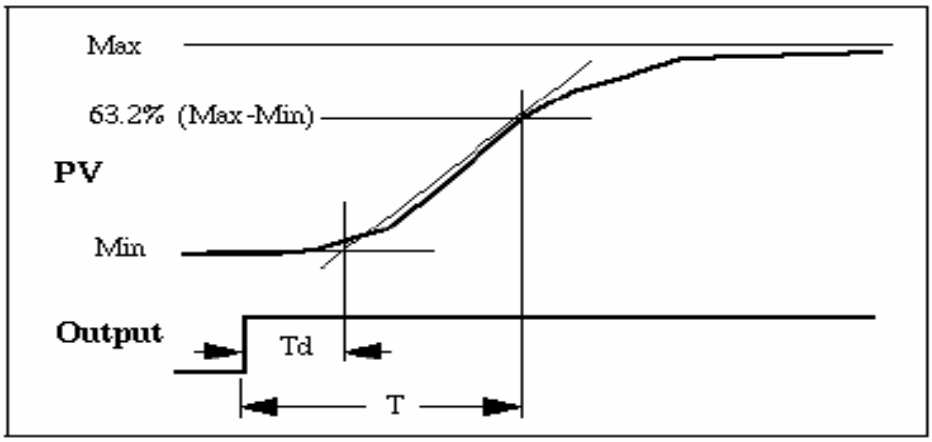

Figure 8. **Output and process variable strip chart (Td-dead time in minutes)**.

Heaters placed throughout the apparatus maintain different parts of the apparatus at specified temperatures. Figure 9 shows the position of the different heaters throughout the apparatus.

Minco thermfoil heaters are used for the isochoric cell temperature control. These thermofoil heaters are simple to apply, yet capable of higher heat output than traditional metal-clad heaters. Kapton insulated heaters have been chosen for this project because of their excellent properties (low out gassing) in high vacuum systems. These heaters provide excellent heat transfer, long life, and uniform heat. The thin film heaters are held in place in the groove with an acrylic heat-shrink film. The copper plate is clamped around the isochoric cell and holds the thermofoil heaters on the bottom and upper isochoric cell in place if the heat shrink should fail.

Table 2. Open Loop Ratios Values

Controller	PB (percent)	Reset (minutes)
P	$100\frac{KT_d}{T}$	-
PI	$110\frac{KT_d}{T}$	$3.33T_d$

Other components included in the control scheme are the KEPCO DC Power supply. Three KEPCO DC power supply (two model ATE 55-5M, one model ATE36-8M) provide the DC power for heater. The KEPCO ATE model output voltage can be

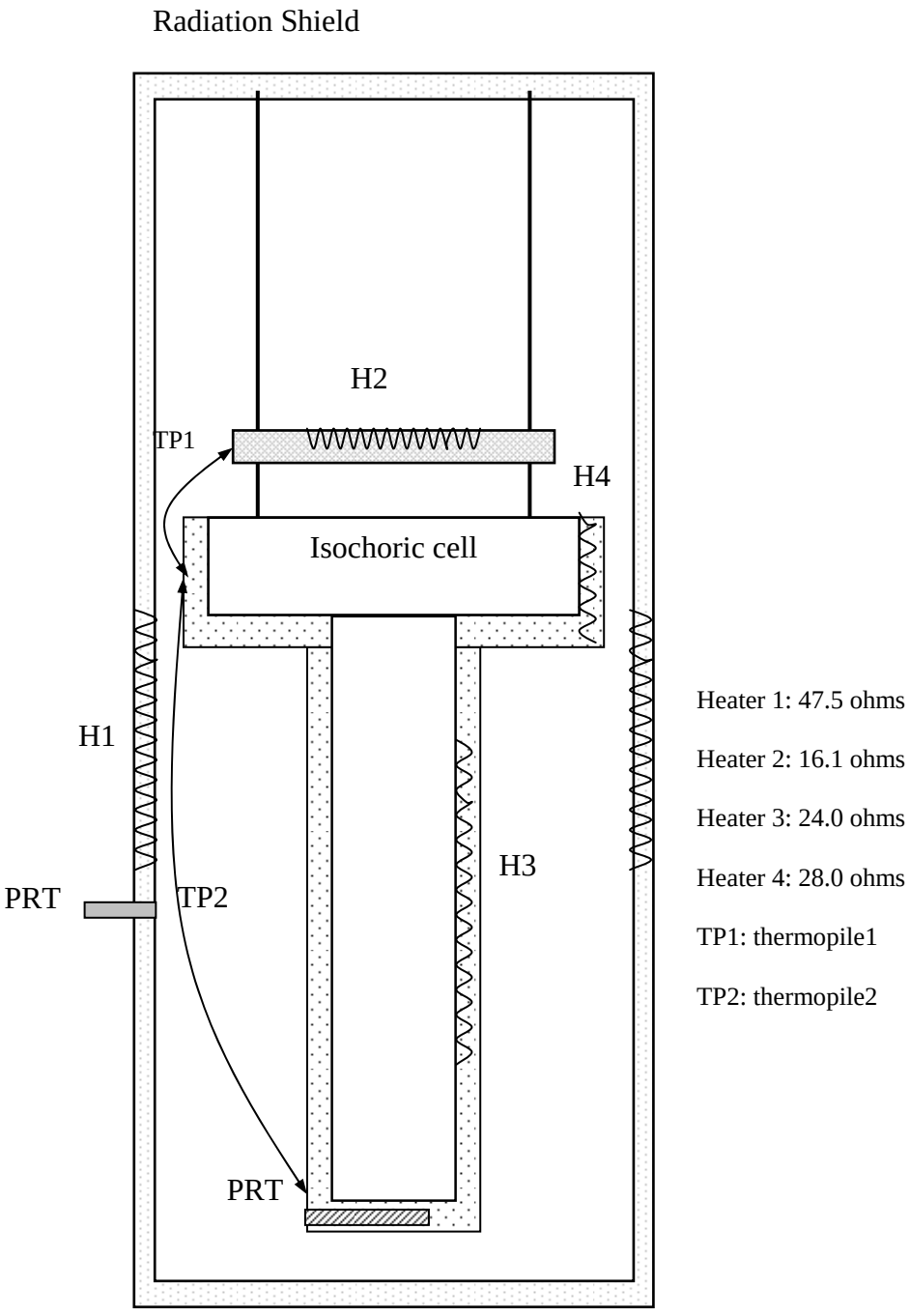

Figure 9. **Location of heaters, thermopiles and PRT through the system.**

controlled remotely by an external 0-10 V analog signal, as long as the external control signal is able to supply at least 1 mA current. The DC power supplies direct voltage in linear proportion to an analog signal of 0 to 10 V from the National Instrument PCI-6704 analog out card. The data acquisition card PCI-6704 is high-resolution (16 bits) analog sources. It can set each output independently from –10 to 10 V or 0 to 20 mA, the voltage output is accurate to 1 mV and current output is accurate to $2\,\mu\text{A}$. This PCI-6704 also is capable of sourcing Transistor-Transistor Logic (TTL) digital signal. This digital signal is capable of reversing current direction in the temperature measurement circuit.

Table 3 shows the PI control parameters used in isochoric cell and isothermal shield temperature control.

Table 3. PID Control Parameters

Heater	PB	Reset
Isochoric Top Section	5	2
Isochoric Bottom Section	5	2
Isothermal Shield (below ambient temperature)	200	180
Isothermal Shield (above ambient temperature)	140	495

This scheme controls all the temperatures to ± 0.004 K. A typical temperature control stability and temperature gradient through the isochoric cell is shown in Figure 10 and Figure 11.

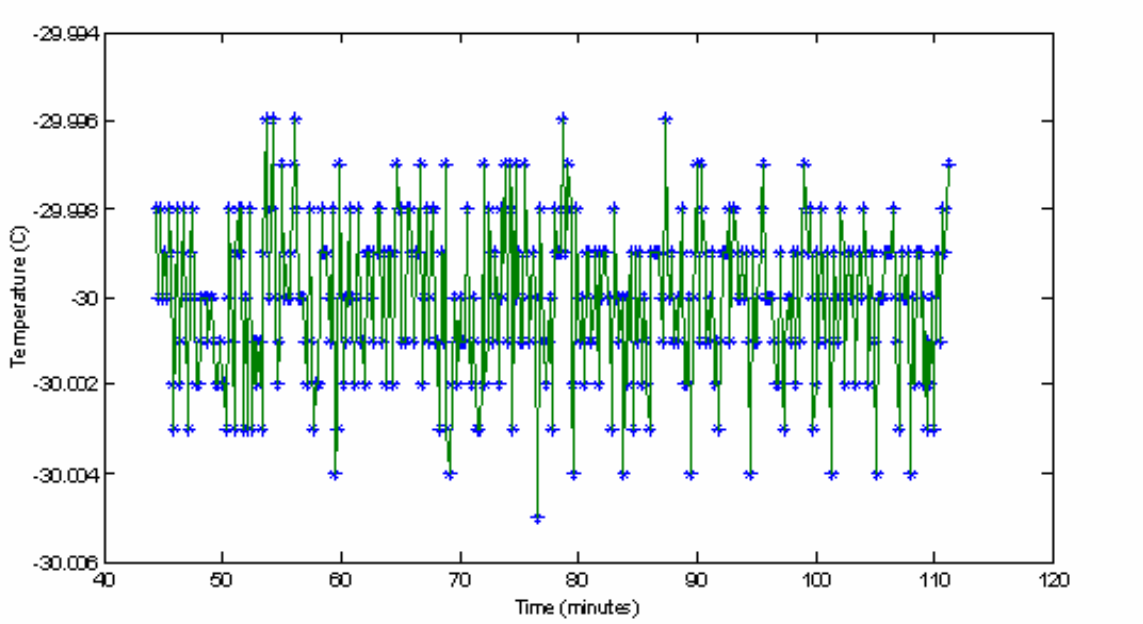

Figure 10. Temperature stability for isochoric cell at T=-30 °C.

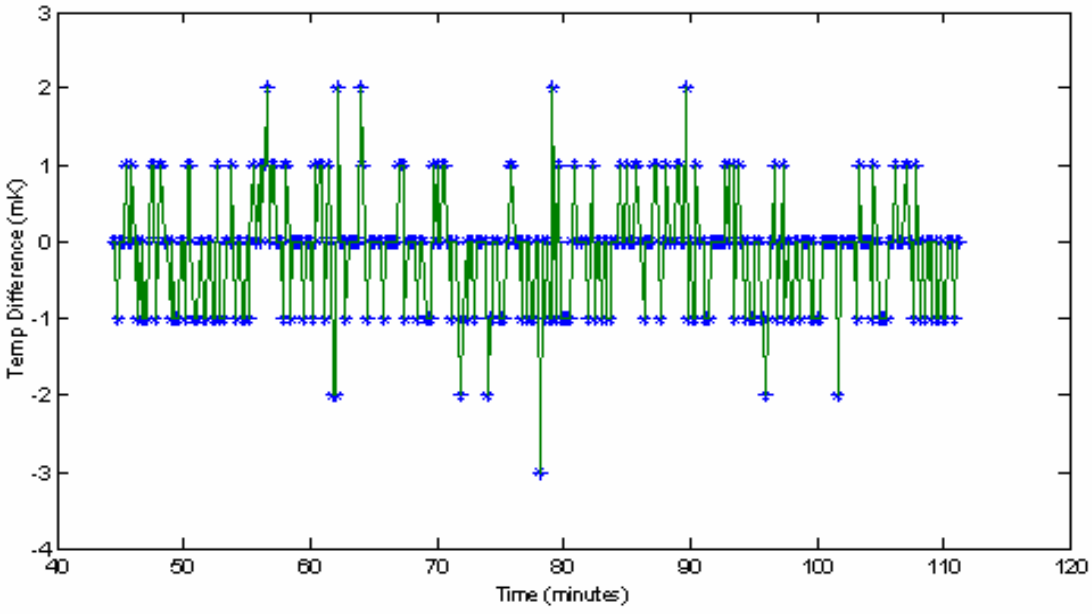

Figure 11. Temperature gradient through isochoric cell at T=-30 °C.

Pressure Measurement

A Paroscientific Inc. pressure transducer is used to measure the isochoric cell pressure. The transducer has a resolution of 0.0001% and typical accuracy of 0.01% full scale. This remarkable performance is achieved using a precision quartz crystal resonator whose frequency of oscillation varies with pressure induced stress. Quartz resonators are chosen for sensing elements because of their chemical inertness and high elasticity. High elasticity means that the mechanical behavior of a material is repeatable from cycle to cycle, and that it is free from hysteresis. Quartz is soluble mainly in fluoride-containing acids and salts. The resonant frequency outputs are detected with oscillator electronics similar to those used in precision clocks and counters (Paroscientific Product Manual, 2004).

Paroscientific Inc. quartz pressure transducer mechanisms employ bellows or Bourdon tubes as the pressure-to-load generators. For low pressures, a quartz beam is attached to a small, hinged metal lever. A bellows is attached to the opposite end of the lever. As the bellows is pressurized, it pushes on the lever, thereby loading the quartz resonator. For high pressures, the resonator is attached across a metal bourdon tube. Pressure applied to the bourdon tube generates an uncoiling force which applies tension to the quartz beam.

Generally, a buffer tube is not required to isolate these transducers from the harmful effects of measured fluids because there is essentially no displacement in the Paroscientific designs, and the bellows/Bourdon tube is so small that there is little fluid movement (Ward and Wiggins, 2004). Mechanical shock, however, can result in a non-

repairable failure of the sensor. A coiled buffer tube is often used as part of the resilient mounting of these transducers to prevent shock or vibration from being transmitted directly to the transducer.

To measure the pressure of the sample, the pressure transducer must have contact with the sample fluid by some direct or indirect manner. In the past, a diaphragm-type differential pressure transducer (DPT) was used to detect sample pressure. An inert fluid was used as an intermediate between the dead-weight gauge and the sample fluid. This technique was successful in generating accurate and reliable data; however the process of determining the equilibrium pressure at a particular point was manual and labor intensive. The automation of pressure the measurement system proved to be difficult because of reliability and safety issues.

The new method used in this project for making pressure measurements involves a “noxious volume” contained within the Paroscientific pressure transducer and the tubing and fittings connecting the pressure transducer to the cell. This noxious volume is not in thermal equilibrium with the sample cell. The noxious volume is at the same temperature as the pressure transducer and at the same pressure as the sample cell.

To reduce this noxious volume in the isochoric cell, the transducer is placed as close to the cell as practical as possible. Unfortunately, we cannot put the transducer inside the vacuum can because the electrical and thermal insulation (silicone rubber) would degas and destroy the vacuum quality. Furthermore, the electronics must be air-cooled or they can heat beyond their operating range, causing possible noise and a loss of accuracy.

Instead, a small bore capillary (ID 0.007 inch, OD 1/16 inch, pressure ratings 6000 psia) connects the isochoric cell to the pressure transducer. By using small ID diameter stainless steel tubing, the noxious volume is reduced greatly. The small bore of the capillary also dramatically reduces gaseous convection between the transducer and cell because the swirling gas movement is impeded by the small diameter of the bore.

To further reduce the noxious volume of the isochoric cell and possible gas condensation, the feed valve is placed inside the isothermal shield and close to the sample cell, allowing the entire confined sample to be subjected to the same uniform temperature. This is especially important when the sample exists as one phase at room temperature and as a different phase at cell temperature.

According to calculations performed by Matabe (1999), so long as the noxious volume represents less than 1% of the cell volume, then the error introduced by the noxious volume has less impact upon the accuracy and precision of the measurements than the thermal expansion of the cell (Matabe, 1999). In this experiment, the approximate noxious volume is about 0.1% of the isochoric cell, about $70\,\mathrm{cm}^3$.

Because the transducer output frequency signal is also affected by transducer temperature, the pressure transducer is mounted in a block of aluminum maintained at a single temperature by SCR and an Omega temperature controller. A PRT mounted in this aluminum block and connected to an Omega temperature controller insures that the pressure transducer is at the proper temperature before taking a measurement. The transducer temperature is maintained at 70 ± 0.02°C. The pressure transducer calibration detail is in Appendix D. Typical pressure stability in isochoric experiment is shown in

Figure 12. The transducer is calibrated against a DH instruments digital dead weight gauge (DWG)-model 26000 to make sure that the pressure data are valid for long term use.

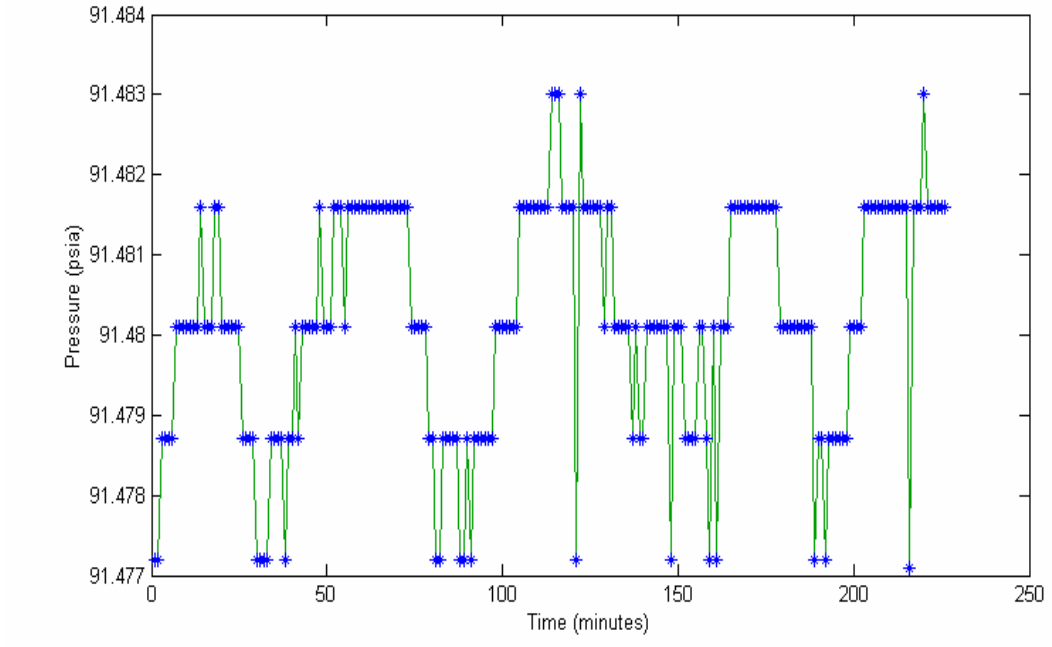

Figure 12. Typical pressure stability monitor in isochoric experiment.

Measurement and Control Programming

In this project, all programming communication with the instrument is written using LabVIEW6.0 from National Instrument (Appendix E). The data are sampled every 10 seconds for temperature measurement and pressure measurement. LabVIEW is a revolutionary graphical development environment with built-in functionality for data acquisition, instrument control, measurement analysis, and data presentation. LabVIEW

delivers seamless connectivity with measurement hardware; the operators can quickly configure and use virtually any measurement device including everything from stand-alone instruments (Keithley DMM2000-20, Paroscientific transducer, Omega temperature controller) to plug-in data acquisition devices (PCI-6704 analog out card, digital out card). The Omega temperature controller is equipped with RS232. There are two ways of communicating with this controller through RS232. The easy way is to use the OPC (open connectivity via open standards) server which can be downloaded from the Omega Inc. website (www.omega.com) or use the Active-X technique. No instrument command is necessary with this technology. The more complex programming technique is to use the instrument command that is available in the Omega communication manual; this programming scheme is more time-consuming.

Another excellent feature of LabVIEW is remote panels control. With this standard feature, the experiment operator can quickly and effortlessly publish the front panel of a LabVIEW program for use in a standard Web browser. Once published, anyone on the Web with the proper permissions can access and control the experiment from the local server. In this project, the LabVIEW program controls isochoric experiment, the remote panels turns the experiment into a remote laboratory with no additional programming or development time.

SAMPLE PREPARATION AND EXPERIMENTAL PROCEDURE

In this chapter, we will briefly discuss the sample preparation and experimental procedure. Both of them are essential for obtaining high accurate experimental data.

Sample Preparation

Pressure-volume-temperature measurements on pure fluids and mixtures are only as precise as their composition. In this study, we have taken great care with sample purification and preparation. Matheson Trigas supplied pure carbon dioxide with a reported purity of 99.995%, and Scott Specialty Gases supplied pure propane with a reported purity of 99.99%. The initial measurements indicated that the propane vapor pressure deviates 0.5% when compared to a NIST 12 (Lemmon et al., 2000) prediction. We suspect that the sample contained volatile impurities. To remove the volatile impurities, we performed repeated cycles of freezing and melting of the gas under vacuum at 150 K in the isochoric cell.

DCG Partnership Inc. and Accurate Gas Product Inc. prepared the four natural gas mixtures with compositions as shown in Tables 4-7.

Table 4. Sample 1 Natural Gas Mixture Compositions

Component	MW (g/mol)	Composition (mol %)
Nitrogen	28.01	2.031
Carbon Dioxide	44.01	0.403
Methane	16.04	90.991
Ethane	30.07	2.949
Propane	44.10	1.513
i-Butane	58.12	0.755
n-Butane	58.12	0.755
i-Pentane	72.15	0.299
n-Pentane	72.15	0.304
Sum	18.20787	100.000

Table 5. Sample 2 Natural Gas Mixture Compositions

Component	MW (g/mol)	Composition (mol %)
Nitrogen	28.01	0.246
Carbon Dioxide	44.01	0.143
Methane	16.04	94.045
Ethane	30.07	1.867
Propane	44.10	1.802
i-Butane	58.12	0.356
n-Butane	58.12	0.706
i-Pentane	72.15	0.201
n-Pentane	72.15	0.252
Hexanes:	86.18	0.205
n-Hexane	86.18	0.199
Methylcyclopentane	84.16	0.006
Heptanes +:		
n-Heptane	100.20	0.100
n-Octane	114.23	0.052
n-Nonane	128.26	0.025
Sum	17.88515	100.000

Table 6. Sample 3 Natural Gas Mixture Compositions

Component	MW (g/mol)	Composition (mol %)
Nitrogen	28.01	0.262
Carbon Dioxide	44.01	0.169
Methane	16.04	88.023
Ethane	30.07	5.824
Propane	44.10	3.292
i-Butane	58.12	0.537
n-Butane	58.12	0.936
i-Pentane	72.15	0.249
n-Pentane	72.15	0.236
Hexanes:	86.18	0.149
n-Hexane	86.18	0.089
2-Methlypentane	86.18	0.045
3-Methlypentane	86.18	0.015
Heptanes +:		
n-Heptane	100.20	0.189
n-Octane	114.23	0.098
n-Nonane	128.26	0.036
Sum	19.15164	100.000

Table 7. Sample 4 Natural Gas Mixture Compositions

Component	MW (g/mol)	Composition (mol %)
Nitrogen	28.01	0.670
Carbon Dioxide	44.01	0.400
Methane	16.04	77.751
Ethane	30.07	10.507
Propane	44.10	5.969
i-Butane	58.12	1.793
n-Butane	58.12	0.992
i-Pentane	72.15	0.495
n-Pentane	72.15	0.495
Hexanes:	86.18	0.534
n-Hexane	86.18	0.218
3-Methlypentane	86.18	0.140
2-Methlypentane	86.18	0.139
Benzene	78.11	0.030
Methylcyclopentane	84.16	0.007
Heptanes:	100.20	0.284
n-Heptane	100.20	0.129
2-methylhexane	100.20	0.050
3-Methylhexane	100.20	0.050
Toluene	92.14	0.035
Methylcyclohexane	98.19	0.020
Octanes:	114.23	0.08
n-Octane	114.23	0.050
2,2,4	114.23	0.030
n-Nonane	128.26	0.030
Sum	-	100.000

Experimental Procedures

We have measured two types of isochores in this study: single phase and two phase. Pure carbon dioxide and propane, loaded from aluminum cylinders, were

calibration and test fluids. The natural gas mixtures were loaded from another aluminum cylinder. A procedure to operate the high pressure isochoric apparatus in the temperature range of 200-500 K is:

1. Heat the isochoric cell, radiation shield and connecting lines to a temperature far above the cricondentherm.
2. Evacuate the isochoric sample cell and the high pressure manifold.
3. Flush the sample cell and lines with sample fluid several times.
4. Charge the gas into the isochoric cell from the sample cylinder.
5. Commence operating the cooling system.
6. Start the control program to drive the temperature of the cell to 4 mK from the set point and the cell gradient to 4 mK. Maintain temperature control until the pressure change cannot be detected by the pressure transducer.
7. Measure an equilibrium point then lower the temperature set point using LabVIEW and the cooling system.
8. Upon reaching the desired temperature, stop cooling isochoric cell and divert all the cooling energy to the isothermal shield. The controller drives the temperature of the cell to the new set point a new equilibrium point is measured. Pressure and temperature is recorded.
9. Repeat steps 6, 7, 8 until reaching the minimum temperature of the two-phase region.

10. After measuring the last point for each isochore, heat the apparatus to the original temperture. Remeasure the original point as a check for possible leaks or composition gradients caused by phase separation.
11. Obtain a new density by releasing a small fraction of the sample fluid into one of the evacuated sections of the inlet tubing, having volumes approximately 5% of the sample volume. Then close the feed valve and repeat the isochoric measurements using the remaining mass of sample. Continue obtaining a desired number of isochors spaced as evenly as possible in density.
12. Measure a new isochore by repeating steps 6-11. Evacuate the cell after measuring the last isochore.

Because the isochoric cell contains no stirring mechanism, it is possible that complete thermodynamic equilibration is never quite reached in the two-phase region. During the initial experimental stage, pressure and temperature readings are recorded both during heating and cooling to check the reproducibility of the measurements. The results are highly reproducible, and therefore, it is reasonable to assume that equilibrium is achieved during the measurements. The experiment shows that 2-3 hours is sufficient to achieve equilibrium in the two-phase regions.

RESULTS AND DISCUSSION

The performance of the isochoric apparatus was confirmed by measuring vapor pressures of pure carbon dioxide and propane. After the performance of the apparatus was verified, isochoric experiments were made on four natural gas mixtures (methane mol %: 91%, 94%, 88%, and 78%).

Carbon Dioxide and Propane Measurement

Equation (12) provided a correction for isochoric volume distortions with changing temperature and pressure. Pure carbon dioxide ($x_{CO_2} > 0.99995$) was used as a calibration fluid. We measured two vapor isochores; the densities along the isochores were calculated using the NIST 12 database (Lemmon et al., 2000). This database provides densities better than $\pm 0.05\%$. A reference density on each isochore was chosen and the volume distortion equation was used to determine the other densities along the isochore. The data in Table 8 show that using equation (12) to correct for volume changes in the cell predicts densities changes along an isochore accurate to about $\pm 0.05\%$.

Measurements on pure carbon dioxide and propane verified the capabilities of the apparatus. Measuring the vapor pressure of a pure substance is a rigorous test of the apparatus because only one degree of freedom exists for a pure fluid in its two phase region. That is to say, a pure fluid in a two-phase region at a given temperature always has the same pressure. It is also a good test of a purification technique because small amounts of volatile impurities have a large effect on the measured vapor pressures.

Table 8. Deviations of Observed Densities Compared to Predicted Densities

Temp (K)	P_{exp} (psia)	$\rho^{(1)}{}_{exp}$ (mol/dm^3)	$\rho^{(2)}{}_{cal}$ (mol/dm^3)	$(\frac{\rho_{exp}-\rho_{cal}}{\rho_{exp}})\times 100$ (%)
		Isochore 1		
315.950	652.565	2.17676[3]		
335.950	719.050	2.17352	2.17286	0.030
355.950	783.818	2.17011	2.16898	0.052
375.950	847.039	2.16599	2.16511	0.041
395.950	909.201	2.16203	2.16125	0.036
415.950	969.565	2.15838	2.15741	0.045
		Isochore 2		
315.950	615.891	2.01828	2.01926	-0.048
335.950	676.511	2.01508	2.01563	-0.027
355.950	735.708	2.01202[3]		
375.950	793.709	2.00879	2.00842	0.018
395.950	850.829	2.00572	2.00483	0.044
415.950	906.925	2.00205	2.00126	0.039

(1) Density calculated with equation 1 and reference density.
(2) Density calculated with NIST database 12.
(3) Data are the reference density for each isochore.

Eight vapor pressures of carbon dioxide measured between 230 K and 290 K showed a maximum deviation of $\pm 0.04\%$ when compared to the NIST 12 Database (Table 9). Seven vapor pressures of propane measured between 270 and 340 K showed a maximum deviation of $\pm 0.07\%$ when compared with the NIST 12 Database (Table 10).

Table 9. Carbon Dioxide Vapor Pressure Compared to NIST 12

Temp (K)	P_{exp} (psia)	P^*_{cal} (psia)	$P_{exp} - P_{cal}$ (psia)	$(\frac{P_{exp} - P_{cal}}{P_{exp}}) \times 100$ (%)
285.350	689.185	689.347	- 0.162	- 0.024
275.350	535.442	535.553	- 0.111	- 0.021
265.550	410.994	411.075	- 0.081	- 0.020
260.550	356.394	356.479	- 0.085	- 0.024
255.550	307.313	307.387	- 0.074	- 0.024
245.950	227.274	227.238	+0.036	+0.016
243.950	212.759	212.699	+0.060	+0.028
235.950	161.237	161.294	- 0.057	- 0.035

*: Calculated from NIST database 12

Table 10. Propane Vapor Pressure Compared to NIST 12

Temp (K)	P_{exp} (psia)	P^*_{cal} (psia)	$P_{exp} - P_{cal}$ (psia)	$(\frac{P_{exp} - P_{cal}}{P_{exp}}) \times 100$ (%)
273.350	69.2594	69.2123	+ 0.047	+ 0.068
275.350	73.5735	73.5307	+ 0.043	+ 0.058
305.650	166.373	166.299	+ 0.074	+ 0.044
310.650	187.247	187.342	- 0.095	- 0.051
320.750	235.841	235.707	+ 0.134	+ 0.057
330.850	292.509	292.665	- 0.156	- 0.053
335.850	324.180	324.346	- 0.166	- 0.051

*: Calculated from NIST database 12

The data in Table 9 and Table 10 also appear in Figure 13.

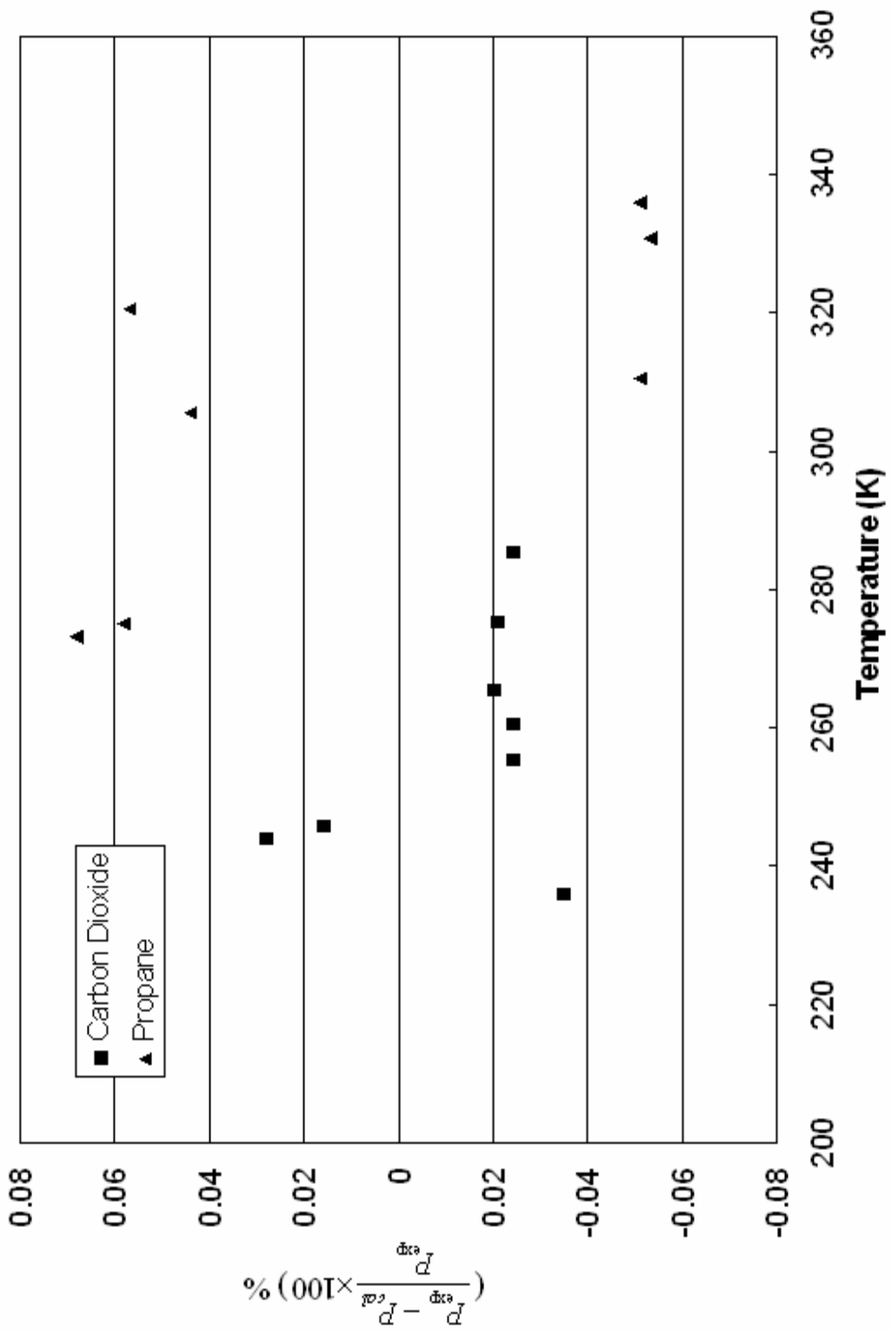

Figure 13. Carbon dioxide and propane vapor pressure comparison with NIST 12.

91% Methane Mixture

For this mixture, ten isochores were measured over a pressure range of 0 to 35 MPa and a temperature range of 220 K to 300 K. The isochoric data for this mixture are in Appendix F. The pressure and temperature data from isochoric experiments have been checked against the density, pressure and temperature data collected on a magnetic suspension densimeter and the comparisons show that the difference between two sets of data is better than 0.1%. This cross-check further shows that the experimental data from isochoric apparatus is reliable and accurate.

Phase Boundary

Table 11 presents the phase boundary data determined for the 91% methane mixture. Several software packages exist for calculating phase envelopes of fluid mixtures. Although these packages may use the Peng-Robsinson (PR) and/or Soave-Redlich-Kwong (SRK) or other EOS, the variations among the packages are such that merely identifying the EOS does not indicate how well they perform. For example, software ProPhy from ProSim Inc. uses the binary interaction parameters from Knapp (1982), while PVTsim from Calsep Inc. assumes the binary interaction parameters are zero and PhasePro from Lomic Inc. uses proprietary binary interaction parameters.

To estimate the accuracy of these commercial software programs in predicting phase envelopes, we compare predictions of phase envelopes using commercial software to experimental data obtained in this project. As seen in Figures 14 and 15, although cubic equations of state can predict the phase equilibrium for hydrocarbon mixtures, they have errors of approximately 1-8% (based upon predictions from PhasePro, same base

with other mixtures) for the 91% mixture dew points. It seems that the SRK equation of state (1-6%) has slightly better performance than PR equation of state (1-8%) in predicting phase envelopes for hydrocarbon mixtures.

Table 11. Phase Envelope of 91% Methane Natural Gas Mixtures

T (K)	P (psia)	P (MPa)
231.8	1274.8	8.789439
239.9	1282.6	8.843218
249.5	1236.3	8.523991
257.2	1138.1	7.846925
267.1	835.4	5.759882
266.1	455.4	3.139873

Several reasons exist for this observation. First, the deviation between the predicted and experimental data is a result of deficiencies in the EOS, such as a constant value of the critical compressibility factor Z_C or inaccurate mixture rules (Twu et al., 2002). Second, and more important, it is a result of the input data. The popular approach in industry to improve the reliability of equations of state is to tune the EOS model using experimental data generated at pertinent conditions for specific field studies. Such an exercise only demonstrates a successful curve fitting. The results for other systems and experimental conditions may be quite disappointing (Danesh, 1998).

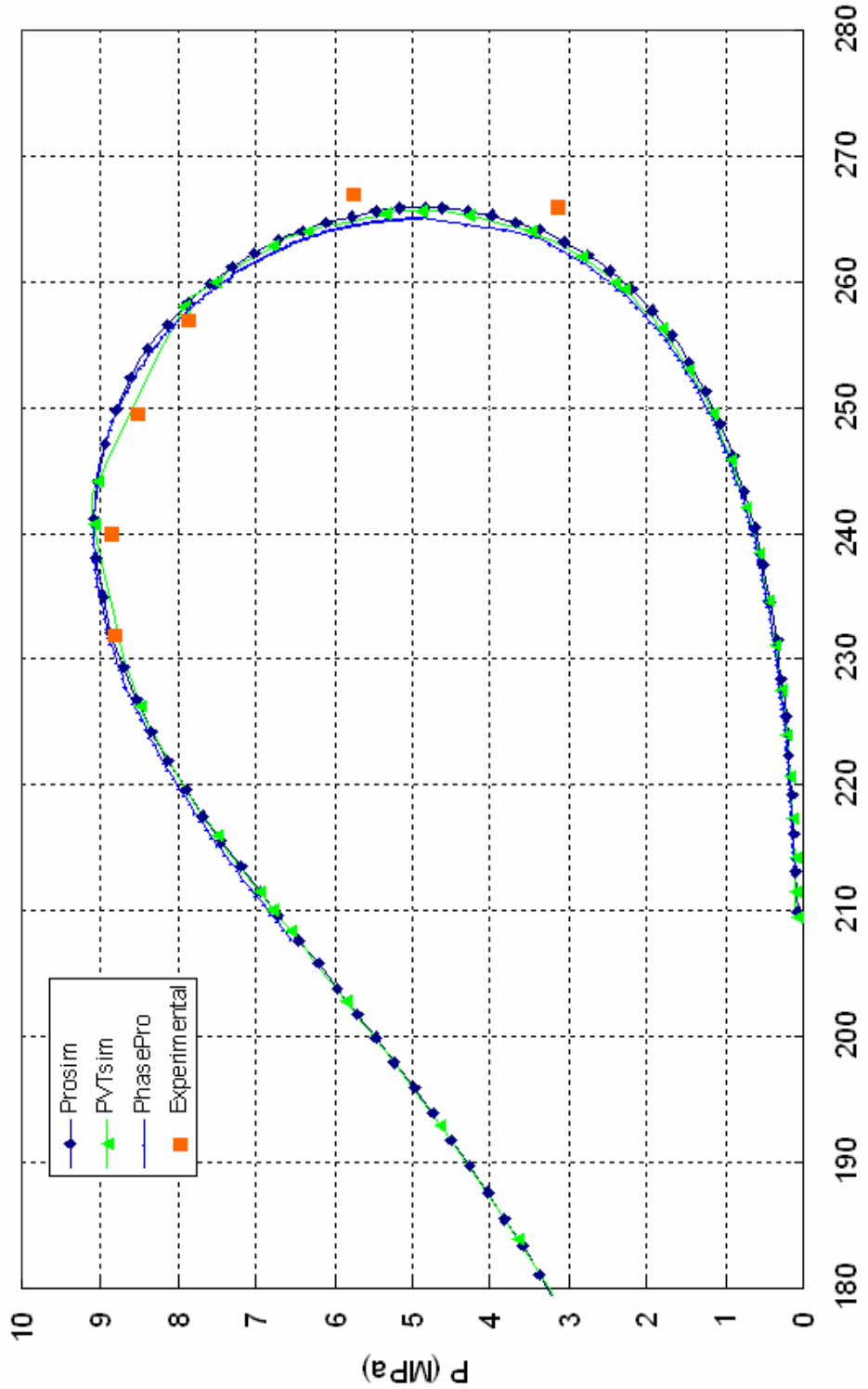

Figure 14. Phase envelope of 91% methane sample comparison with SRK equation.

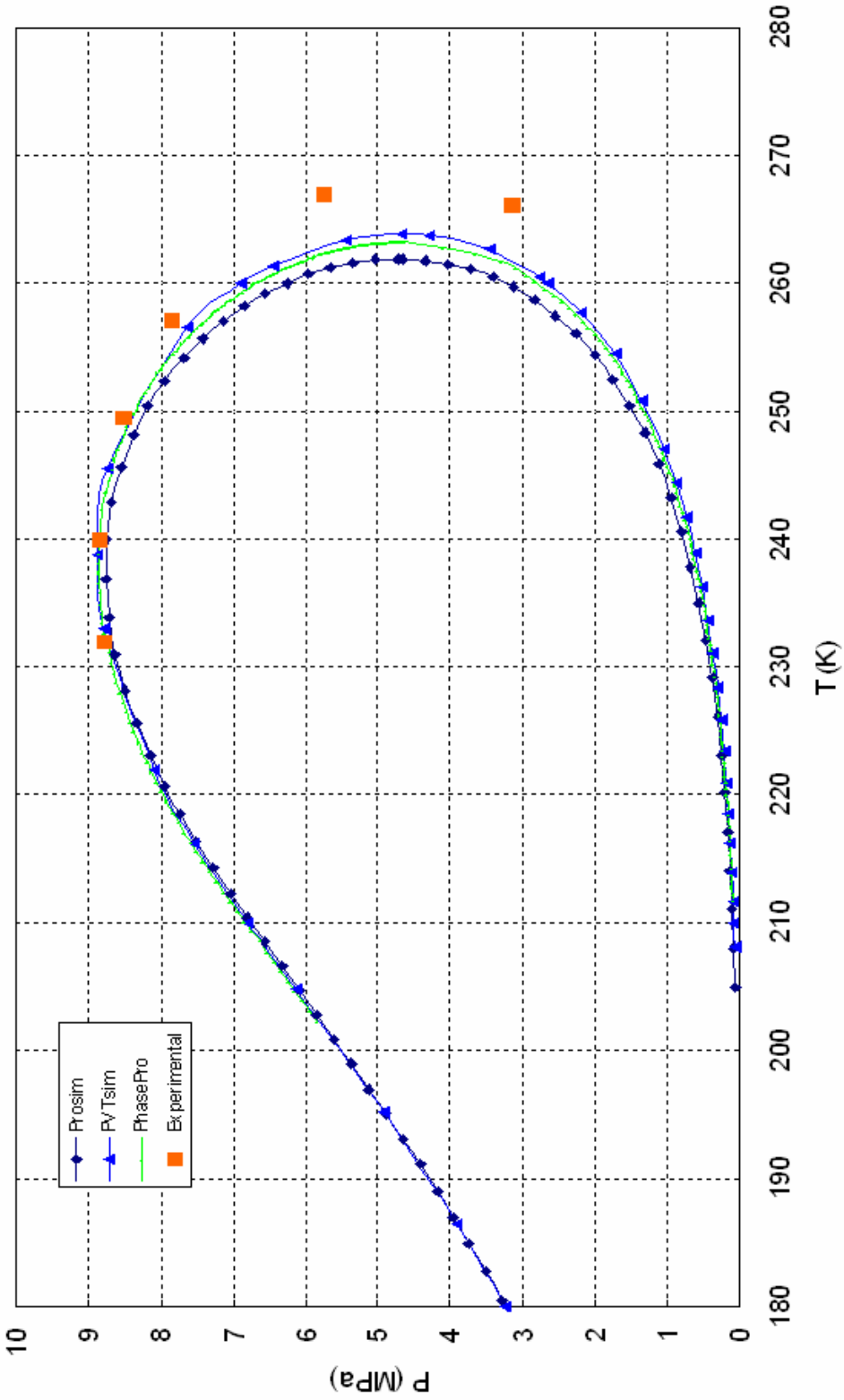

Figure 15. Phase envelope of 91% methane sample comparison with PR equation.

Density

Figure 16 shows mixture densities obtained from isochoric experiments and those calculated from AGA 8-DC92 equation of state. The comparison illustrates that AGA8-DC92 has errors ranging from -0.64% to +0.19% when predicting mixture densities. AGA8-DC92 claims to have $\pm 0.1\%$ accuracy in predicting natural gas mixture densities in applicable ranges of temperature, pressure and composition, but the development of AGA8-DC92 is based upon fitting very limited multicomponent mixture data. In addition, its validity is doubtful when extrapolating the temperature, pressure or composition range. Although the 91% methane mixture composition falls within the expanded range of AGA8-DC9, it is not in the normal composition range for this equation. This explains why AGA8-DC92 performs poorly when predicting densities for this mixture. The experimental densities from this project provide an excellent source of data to develop of this equation of state further. A new equation of state is under development in our group.

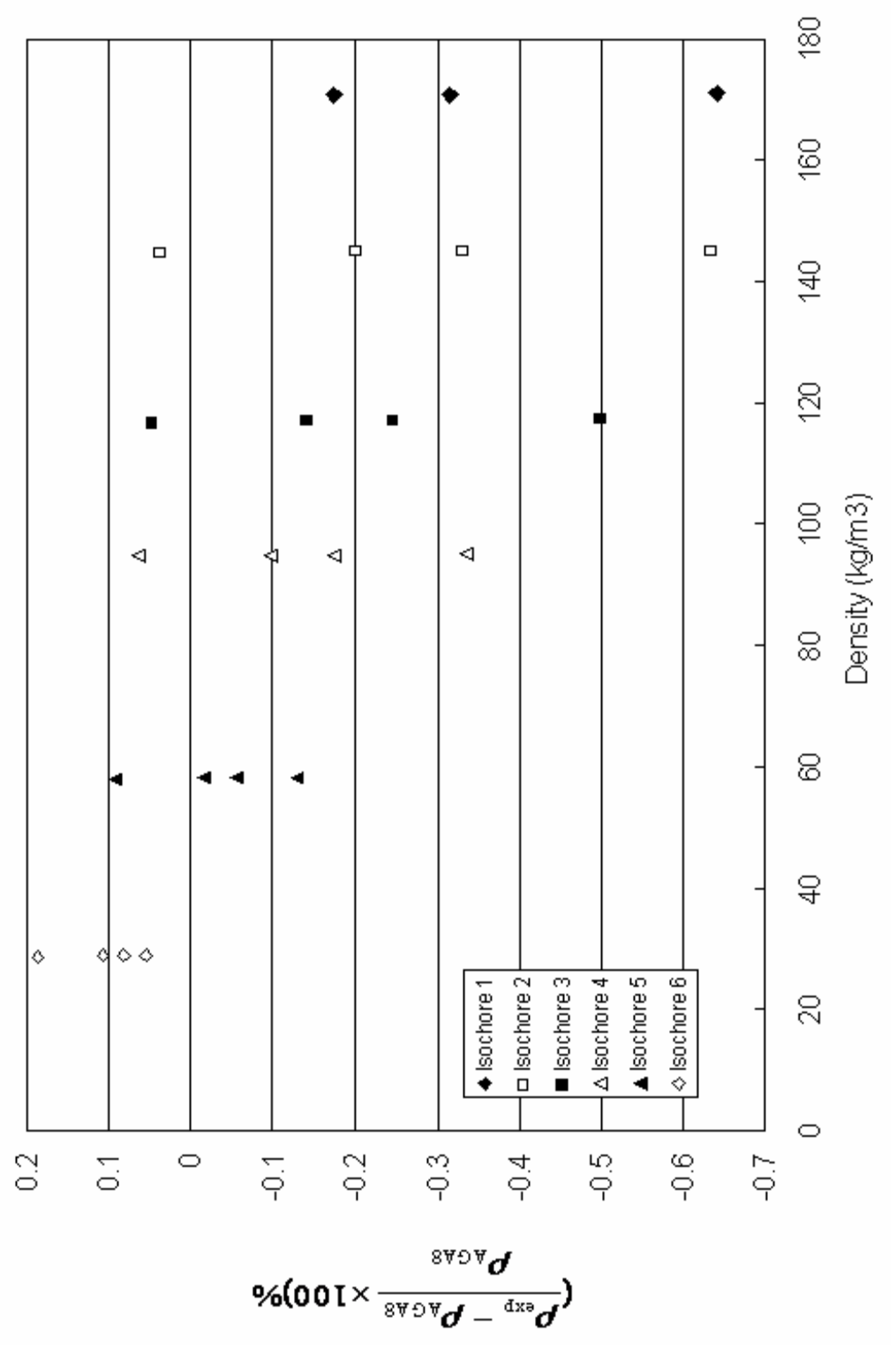

Figure 16. Density of 91% methane sample comparison with AGA8 equation of state.

The detailed density data are shown in Table 12.

Table 12. Density of 91% Methane Natural Gas Mixtures

T	P	ρ_{exp} (1)	ρ_{cal} (2)	$(\frac{\rho_{exp} - \rho_{cal}}{\rho_{exp}}) \times 100$
(K)	(MPa)	(kg/m3)	(kg/m3)	(%)
		Isochore 1		
305.15	18.884808	170.734	171.029	-0.17
290.65	16.892637	170.863	171.404	-0.32
270.15	14.063097	171.046	172.145	-0.64
		Isochore 2		
340.15	19.660606	144.851	144.797	0.04
305.15	15.936334	145.111	145.405	-0.20
290.65	14.372534	145.219	145.701	-0.33
270.15	12.146838	145.372	146.294	-0.63
		Isochore 3		
340.15	15.790166	117.001	116.945	0.05
305.15	13.029780	117.208	117.375	-0.14
290.65	11.869531	117.294	117.584	-0.25
270.15	10.214582	117.416	118.005	-0.50
		Isochore 4		
340.15	12.873201	94.638	94.576	0.06
305.15	10.790363	94.803	94.894	-0.10
290.65	9.9137642	94.872	95.037	-0.17
270.15	8.6597458	94.970	95.289	-0.34
		Isochore 5		
340.15	8.1556012	57.952	57.898	0.09
305.15	7.0229305	58.052	58.061	-0.02
290.65	6.5463649	58.094	58.126	-0.06
270.15	5.8650664	58.153	58.228	-0.13
		Isochore 6		
340.15	4.2210250	28.747	28.693	0.19
305.15	3.7156397	28.797	28.766	0.11
290.65	3.5036879	28.817	28.793	0.08
270.15	3.2013598	28.846	28.830	0.06

(1): Experimental density from isochoric apparatus.
(2): Density calculated with AGA8-DC92 equation of state.

94% Methane Mixture

For this mixture, we have measured ten isochores over a pressure range of 0 to 35 MPa and a temperature range of 220 K to 300 K. The isochoric data for this mixture are in Appendix G. The pressure and temperature data from the isochoric experiments have been checked against the density, pressure and temperature data collected with a magnetic suspension densimeter and the comparisons show that the difference between two sets of data is less than 0.1%.

Phase Boundary

Table 13 presents the phase boundary data determined for the 94% methane mixture. The phase diagram with experimental points compared to Peng-Robinson and Soave–Redlich–Kwong appears as Figures 17 and 18. The two figures show that the cubic equations of state have approximate 1-16% error in predicting 94% methane mixture dew points. The SRK equation of state (1-9%) appears to perform better than the PR equation of state (2-16%) when predicting hydrocarbon mixture phase envelopes.

Table 13. Phase Envelope of 94% Methane Natural Gas Mixtures

T (K)	P (psia)	P (MPa)
235.99	1396.0	9.625080
247.42	1499.6	10.33937
258.88	1545.8	10.65791
270.14	1542.1	10.63240
289.50	1404.0	9.680238
294.97	1284.4	8.855625
298.64	1162.3	8.013776
303.71	932.15	6.426948
304.52	459.66	3.169244
294.03	188.47	1.299455

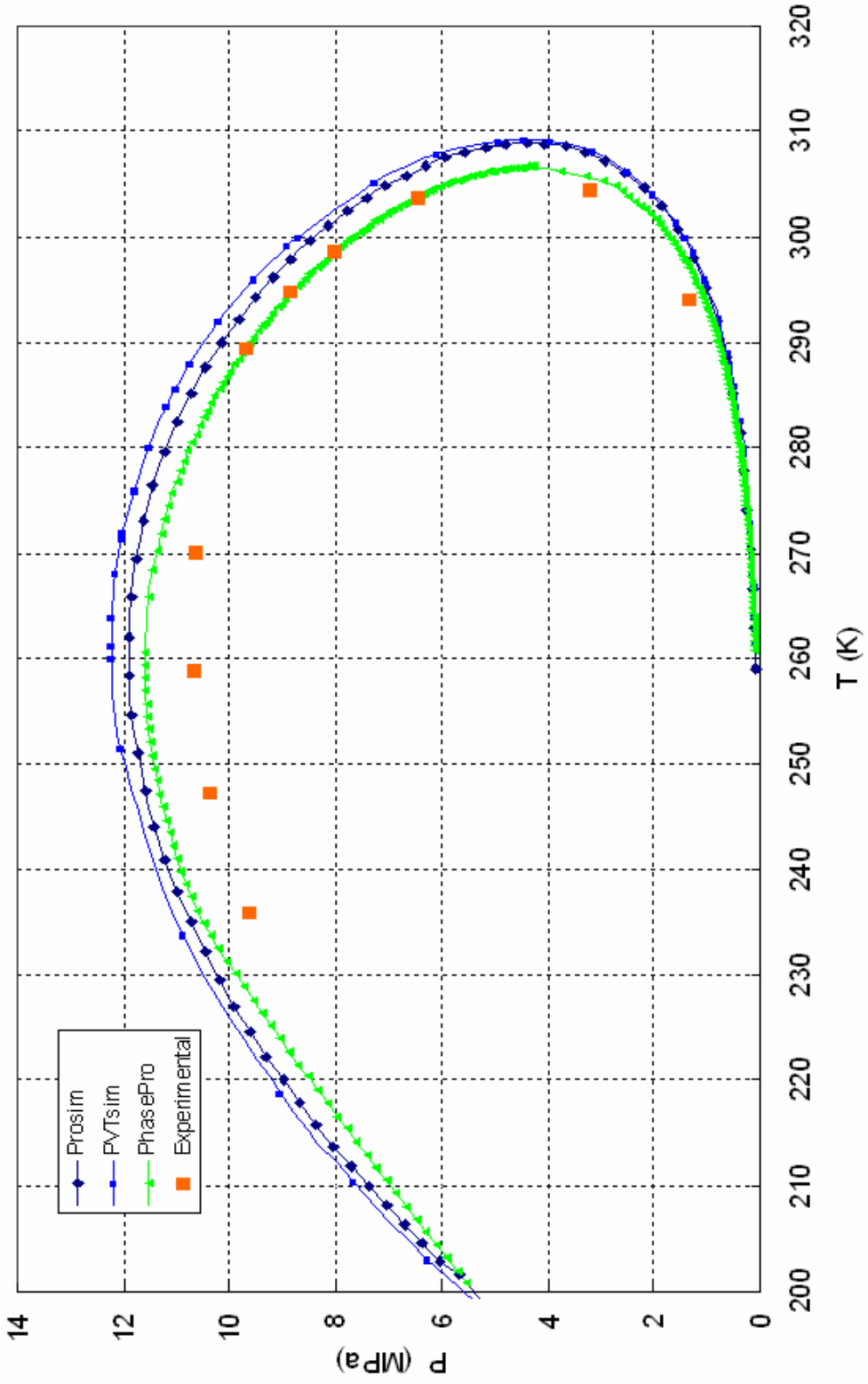

Figure 17. Phase envelope of 94% methane sample comparison with SRK equation.

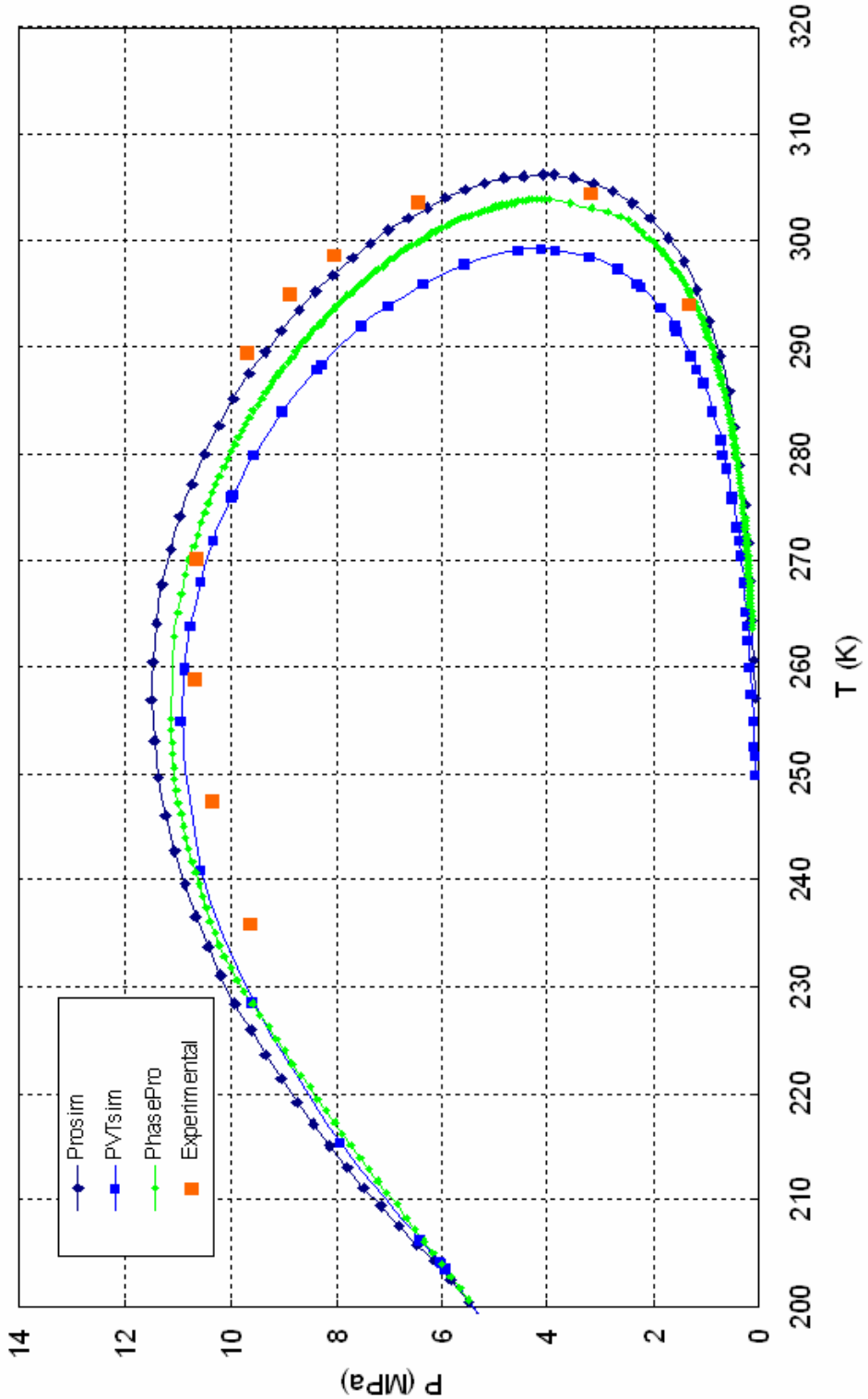

Figure 18. Phase envelope of 94% methane sample comparison with PR equation.

Density

Table 14 shows mixture densities obtained from the isochoric experiment and those calculated from AGA 8-DC92. The comparison shows that AGA8-DC92 has errors ranging from -0.20% to +0.28% in calculating densities for this mixture. Again, this can be explained because the 94% natural gas mixtures composition is not in the normal range for AGA8-DC92.

Table 14. Density of 94% Methane Natural Gas Mixtures

T (K)	P (MPa)	$\rho_{\exp}$ (1) (kg/m3)	ρ_{cal} (2) (kg/m3)	$(\frac{\rho_{\exp}-\rho_{cal}}{\rho_{\exp}})\times 100$ (%)
		Isochore 1		
301.150	19.28802	175.964	175.629	0.19
286.450	17.11431	176.101	175.803	0.17
277.950	15.84747	176.177	175.822	0.20
266.950	14.2121	176.280	175.855	0.24
261.950	13.46898	176.326	175.841	0.28
		Isochore 2		
301.150	17.04426	157.000	156.860	0.09
287.750	15.37786	157.109	156.987	0.08
279.950	14.40398	157.172	157.046	0.08
267.950	12.90347	157.269	157.123	0.09
261.950	12.15849	157.319	157.231	0.06
		Isochore 3		
313.350	16.3383	138.875	138.627	0.18
306.350	15.61615	138.925	138.693	0.17
301.350	15.09904	138.960	138.741	0.16
289.450	13.86605	139.045	138.881	0.12
277.950	12.66374	139.127	138.960	0.12
		Isochore 4		
333.350	16.03142	121.178	120.951	0.19
323.350	15.18619	121.241	121.035	0.17
313.350	14.33717	121.301	121.123	0.15
303.350	13.48401	121.362	121.214	0.12
290.450	12.37837	121.442	121.352	0.07

Table 14. (Continued)

T (K)	P (MPa)	ρ_{exp} (1) (kg/m3)	ρ_{cal} (2) (kg/m3)	$(\frac{\rho_{exp}-\rho_{cal}}{\rho_{exp}})\times 100$ (%)
		Isochore 5		
335.450	12.3703	91.275	91.222	0.06
325.350	11.78556	91.321	91.291	0.03
315.350	11.20316	91.368	91.358	0.01
305.350	10.618	91.413	91.432	-0.02
292.950	9.88936	91.470	91.547	-0.08
		Isochore 6		
335.450	10.82091	78.899	78.978	-0.10
327.050	10.41702	78.931	79.033	-0.13
320.150	10.08276	78.958	79.069	-0.14
313.150	9.74326	78.985	79.114	-0.16
305.150	9.353706	79.017	79.168	-0.19
		Isochore 7		
335.450	9.514216	68.710	68.685	0.04
327.150	9.178648	68.738	68.731	0.01
320.150	8.894101	68.762	68.768	-0.01
313.150	8.60852	68.786	68.805	-0.03
305.150	8.281433	68.814	68.854	-0.06
		Isochore 8		
335.450	7.348296	51.836	51.893	-0.11
327.150	7.108841	51.857	51.927	-0.13
320.150	6.90586	51.874	51.954	-0.15
313.150	6.702244	51.893	51.981	-0.17
305.150	6.469125	51.913	52.018	-0.20

The comparison of experimental data with AGA8 is shown in the Figure 19.

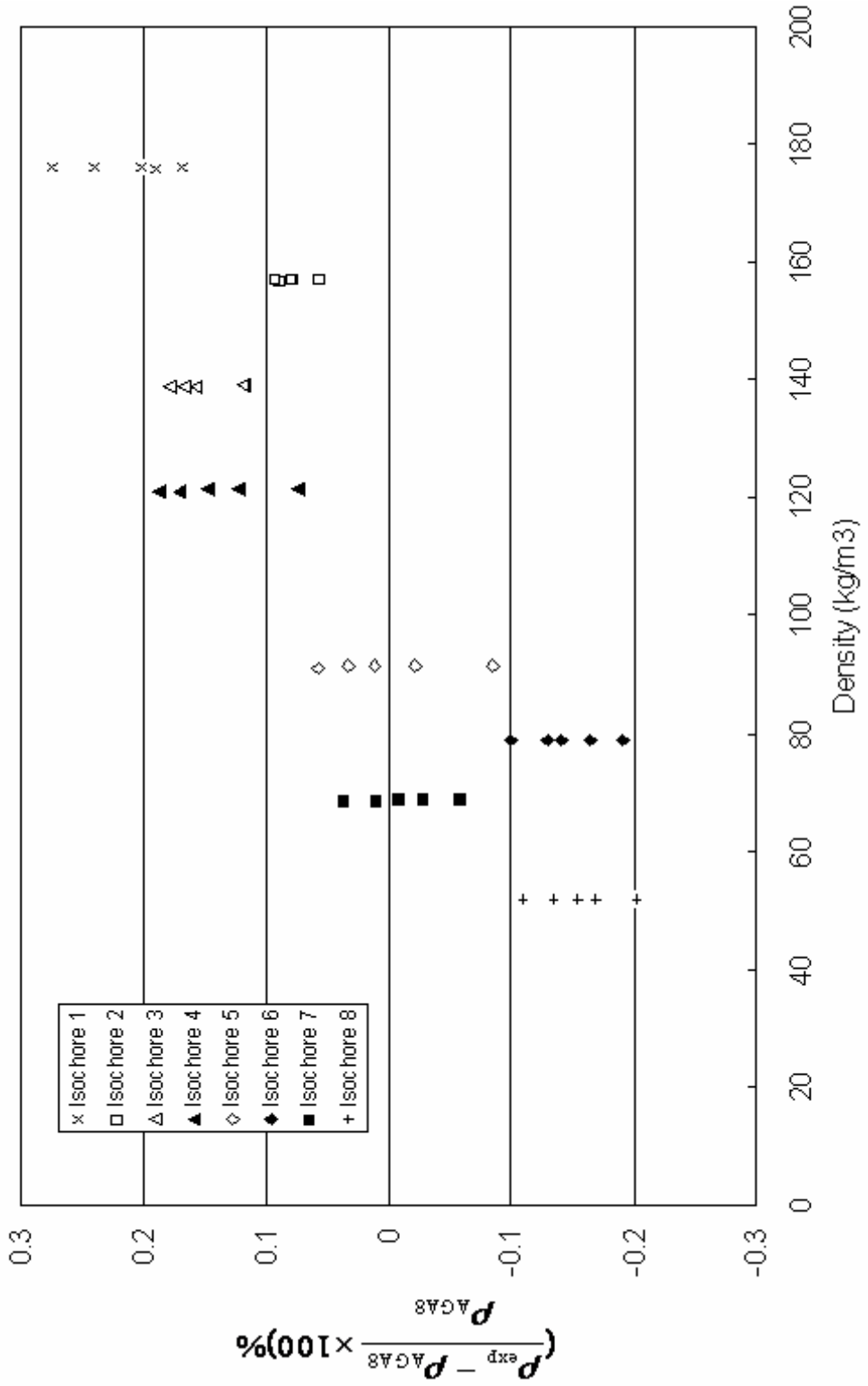

Figure 19. Density of 94% methane sample comparison with AGA8 equation of state.

88% Methane Mixture

For this mixture, ten isochores have been measured over a pressure range of 0 to 35 MPa and a temperature range of 220 K to 300 K. The isochoric data for this mixture are in Appendix H. The pressure and temperature data from the isochoric experiment have been checked against the density, pressure and temperature data from a magnetic suspension densimeter and the comparisons show that the difference between two sets of data is less than 0.1%.

Phase Boundary

Table 15 presents the phase boundary data measured for the 88% methane mixture. The phase diagram with experimental points is compared to the Peng-Robinson and Soave–Redlich–Kwong EOS in Figures 20 and 21. As seen from the figures, the cubic equation of state has approximate 1-12% error in predicting the dew points. For this mixture, the PR equation of state (1-8%) performs better than the SRK equation of state (1-12%) in predicting the hydrocarbon mixture phase envelope.

Table 15. Phase Envelope of 88% Methane Natural Gas Mixtures

T (K)	P (psia)	P (MPa)
255.5	1619.8	11.16813
261.7	1662.0	11.45909
273	1686.5	11.62801
284.4	1671.3	11.52321
293.6	1591.9	10.97577
305.4	1330.0	9.17003
308.8	1191.7	8.216484
310.7	1053.7	7.265008
313.0	756.3	5.214506
305.0	236.4	1.629921

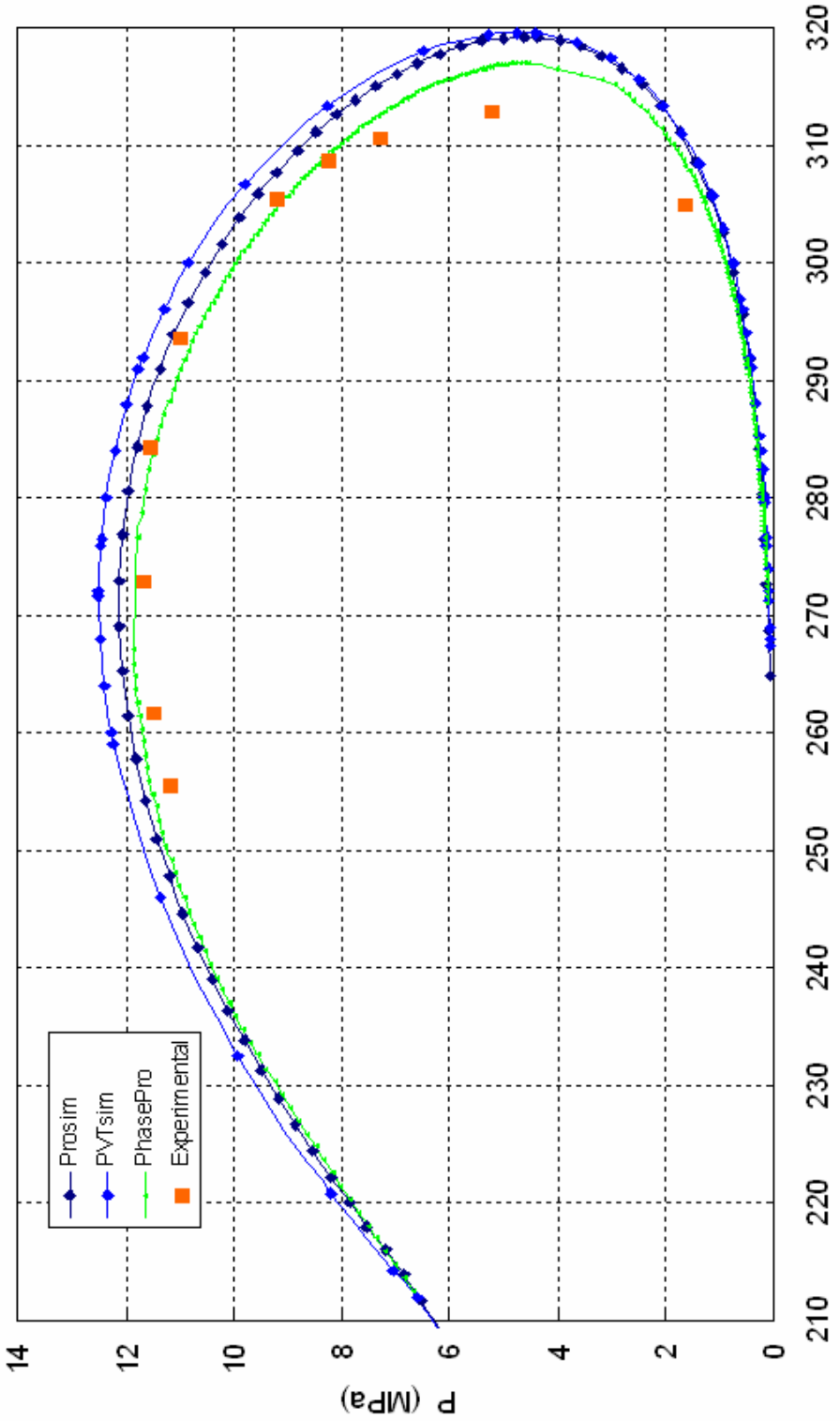

Figure 20. Phase envelope of 88% methane sample comparison with SRK equation.

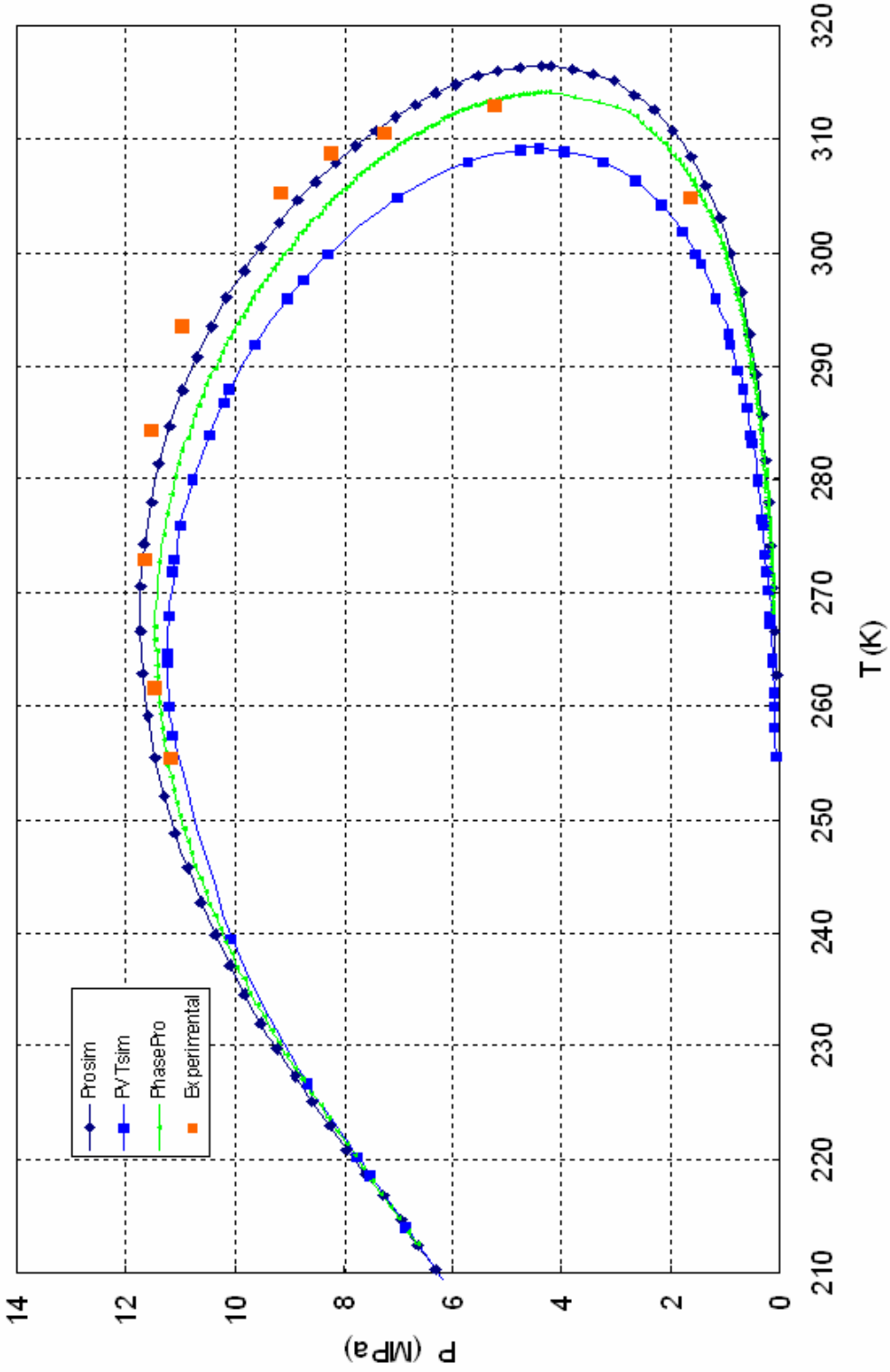

Figure 21. Phase envelope of 88% methane sample comparison with PR equation.

Density

Table 16 presents mixture densities obtained from isochoric experiments and those calculated from AGA 8-DC92. The comparison shows that AGA8-DC92 has errors ranging from -0.37% to +0.48% in calculating densities for this mixture. Again, this can be explained because the 88% mixture composition is not in normal range of AGA8-DC92.

Table 16. Density of 88% Methane Natural Gas Mixtures

T (K)	P (MPa)	ρ_{exp} [1] (kg/m3)	ρ_{cal} [2] (kg/m3)	$(\frac{\rho_{exp}-\rho_{cal}}{\rho_{exp}})\times 100$ (%)
		Isochore 1		
302.050	18.12377	186.034	185.500	0.29
287.650	15.97143	186.173	185.549	0.34
280.650	14.92467	186.242	185.537	0.38
274.650	14.02649	186.301	185.472	0.44
270.650	13.43154	186.340	185.444	0.48
		Isochore 2		
311.150	18.18424	174.984	174.592	0.22
303.150	17.09921	175.058	174.641	0.24
293.150	15.74122	175.149	174.694	0.26
283.150	14.38123	175.239	174.712	0.30
275.150	13.29254	175.312	174.675	0.36
		Isochore 3		
320.150	16.91822	153.893	153.699	0.13
308.350	15.60153	153.985	153.782	0.13
302.150	14.90716	154.035	153.819	0.14
293.150	13.89811	154.106	153.880	0.15
283.150	12.77302	154.186	153.919	0.17
		Isochore 4		
328.950	15.63973	134.726	134.472	0.19
320.150	14.83256	134.786	134.531	0.19
308.150	13.7296	134.869	134.640	0.17
302.650	13.22008	134.906	134.669	0.18
293.150	12.33865	134.972	134.735	0.18

Table 16. (Continued)

T (K)	P (MPa)	ρ_{exp} [1] (kg/m3)	ρ_{cal} [2] (kg/m3)	$(\frac{\rho_{exp}-\rho_{cal}}{\rho_{exp}})\times 100$ (%)
		Isochore 5		
338.950	14.40405	116.763	116.543	0.19
328.950	13.65445	116.823	116.605	0.19
320.150	12.99262	116.874	116.669	0.18
308.150	12.08513	116.946	116.758	0.16
300.150	11.47577	116.992	116.807	0.16
		Isochore 6		
342.450	5.855967	42.845	42.990	-0.34
329.150	5.565401	42.872	43.014	-0.33
325.150	5.478638	42.881	43.029	-0.35
321.150	5.391481	42.889	43.043	-0.36
316.150	5.282323	42.901	43.060	-0.37

The comparison of experimental data with AGA8 is shown in the Figure 22.

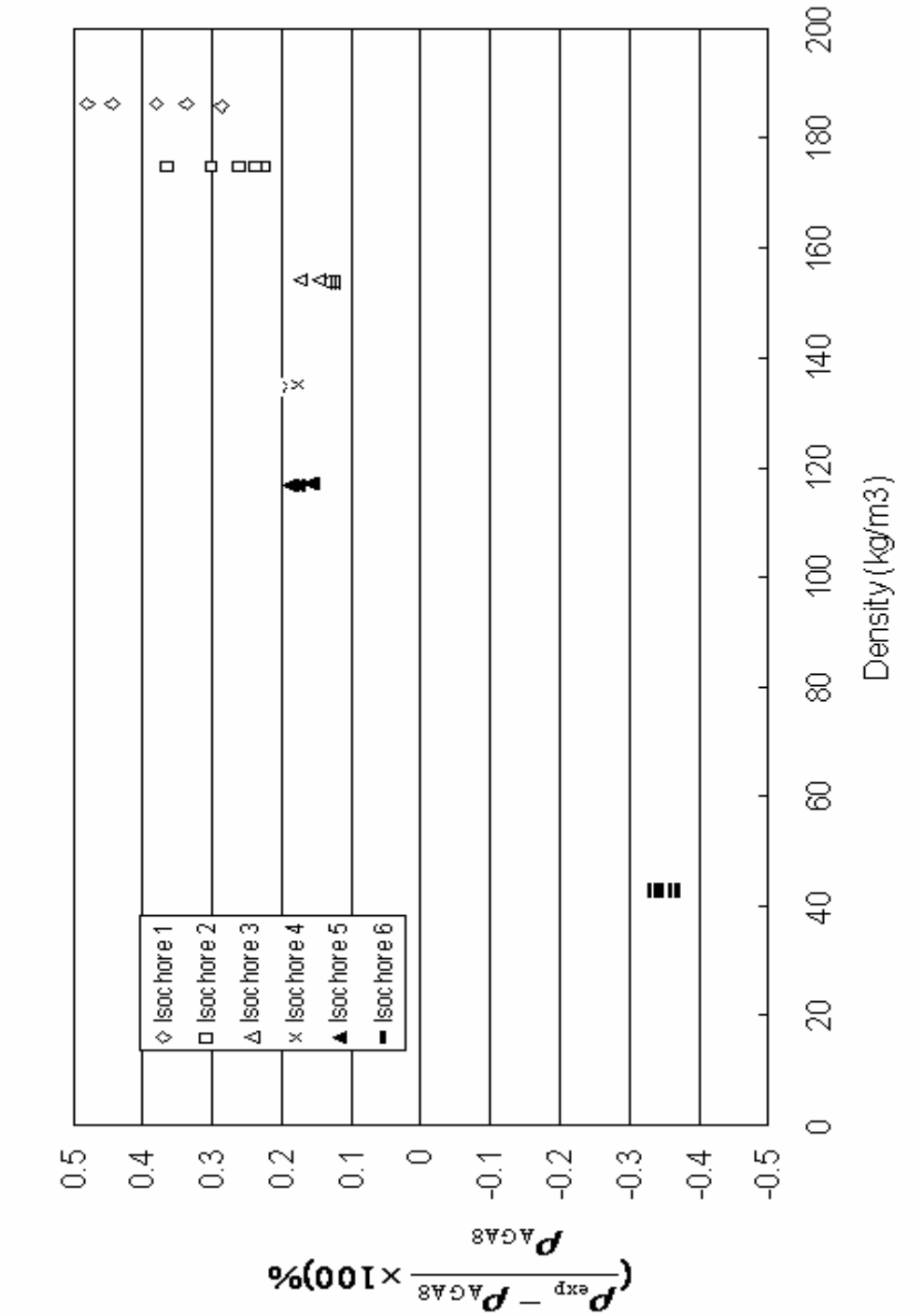

Figure 22. Density of 88% methane sample comparison with AGA8 equation of state.

78% Methane Mixture

For this mixture, we have measured ten isochores over a pressure range of 0 to 35 MPa and a temperature range of 220 K to 300 K. The isochoric data for this mixture are in Appendix I.

Phase Boundary

Table 17 presents the phase boundary data determined for 78% methane mixture. The phase diagram with experimental points is compared to the Peng-Robinson and Soave–Redlich–Kwong EOS in Figures 23 and 24. As seen from the Figures, the cubic equations of state have approximately 1-18% errors in predicting the 78% mixture dew points. The PR equation of state (1-4.4%) performs better than the SRK equation of state (4-18%) in predicting the phase envelope.

Table 17. Phase Envelope of 78% Methane Natural Gas Mixtures

T (K)	P (psia)	P (MPa)
325.1	517.8	3.57011
322.5	1050.3	7.24157
313.9	1355.8	9.34791
302.1	1574.5	10.8558
286.5	1657.0	11.4246
275.5	1660.6	11.4494
264.5	1619.5	11.1661

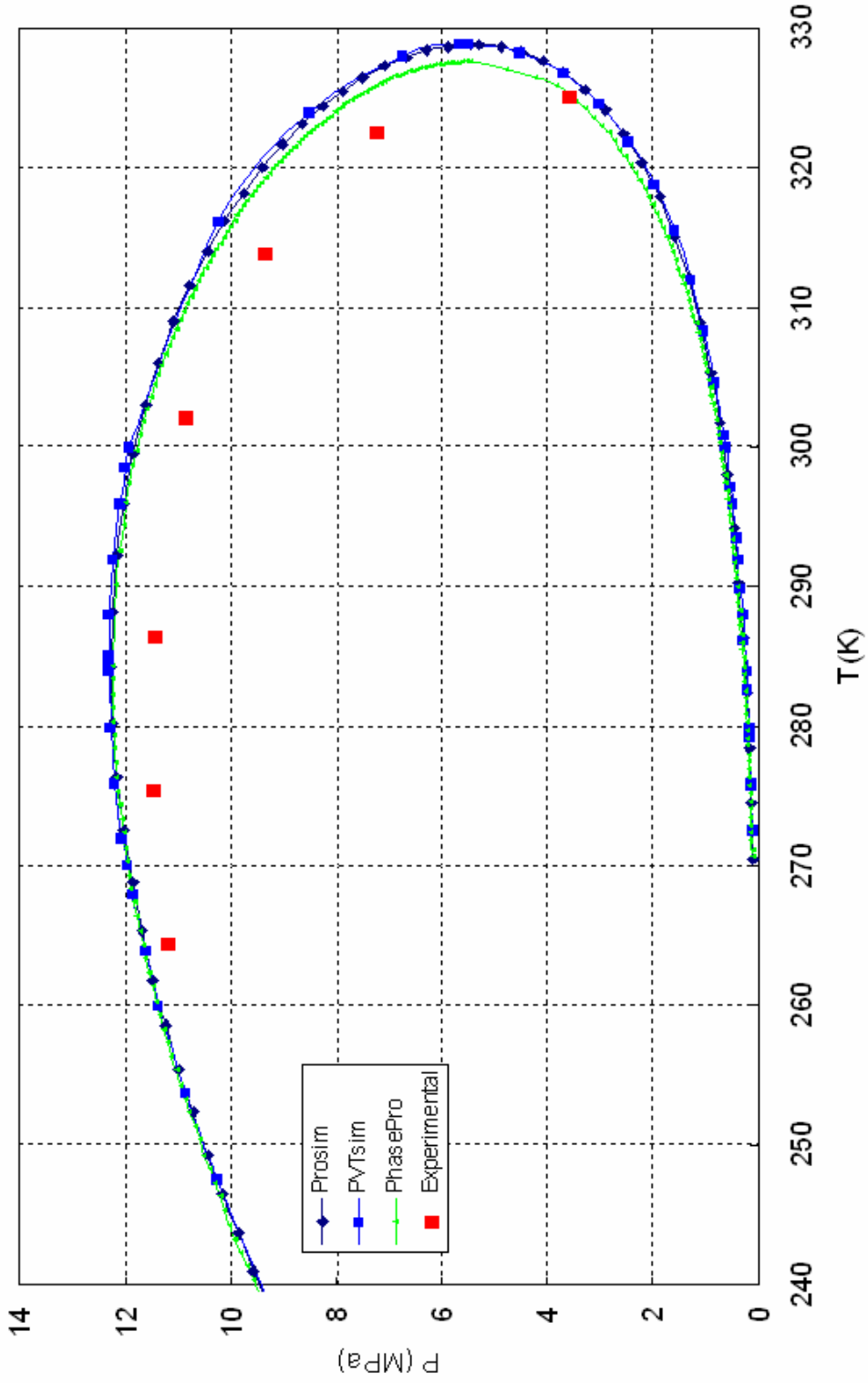

Figure 23. Phase envelope of 78% methane sample comparison with SRK equation.

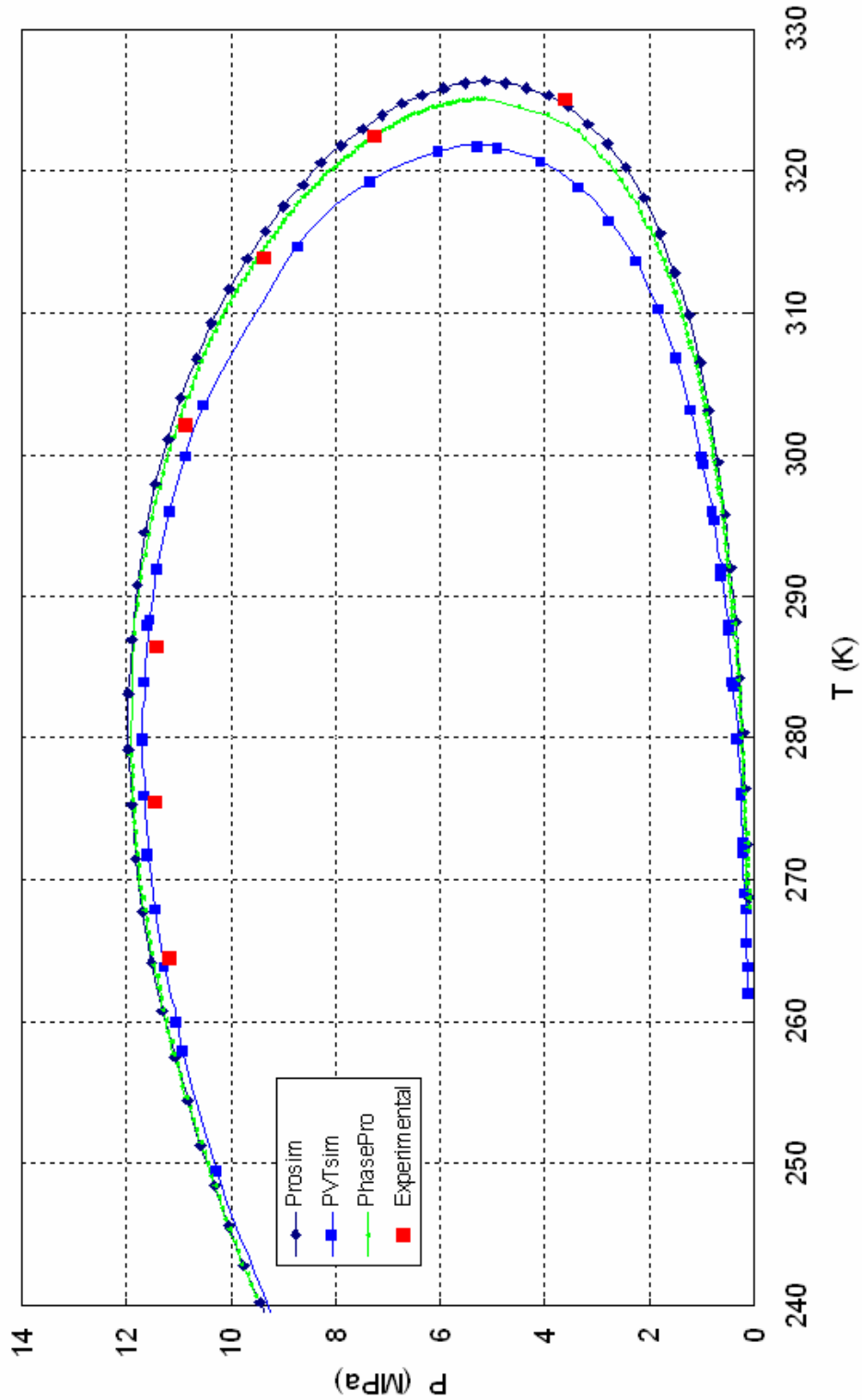

Figure 24. Phase envelope of 78% methane sample comparison with PR equation.

Density

The density data for this sample are not available because of a delay in density measurements using magnetic suspension densimeter.

Error Analysis

This section presents an estimate of the errors in the phase boundary and density measurements.

Phase Boundary

The two major errors in the phase boundary determinations are: errors in the temperature and pressure measurements and errors involved with determining the intersection point (phase boundary) of the single phase and the two phase isochores. The accuracy of the temperature and pressure measurements is 0.01 K and 0.002 MPa respectively. These small errors in pressure and temperature measurements are negligible in phase boundary determinations.

The phase boundary determination accuracy can be estimated by the standard deviation (standard error) of equation (10). The largest deviation from the intersection point of the original fit is an estimate of the error in determining the phase boundary. As a result, we estimate the phase boundary data to be within 0.5 K (95% confidence level) in temperature and 0.2% in pressure.

It should be mentioned here that the determination of the isochoric intercepts involves an extrapolation of each p-T quasi-isochore because these measurements are not made exactly up to the vapor-liquid phase boundary. This introduces additional

errors in temperature and pressure at the points of intersection which are not considered in the above error analysis and which are very difficult to estimate.

Density

The major errors in the density determinations are the errors from measuring the original densities and the errors introduced by the cell distortion corrections. The original densities from the magnetic suspension densimeter have $\pm 0.05\%$ accuracy. The cell distortion correction introduces an error of $\pm 0.05\%$ in density. We have no estimate of the deformation of the transducer volume with pressure, but we have assumed it to be approximately the same as that of the isochoric vessels. Because the transducer contains only about 0.1% of the sample in the isochoric runs, even an error of a factor of 10 in its pressure deformation would not lead to appreciable density errors. Based upon the above information, isochoric density measurement errors are estimated to be less than $\pm 0.1\%$.

CONCLUSIONS AND RECOMMENDATIONS

We have designed and built a high-pressure isochoric apparatus for fast and accurate *PVT* and phase equilibrium measurements. The apparatus can measure isochoric data for fluids over a wide range of pressure (0-35 MPa) and temperature (200-500 K). Temperature measurements are accurate to 10 mK on IPTS-90 and precise to 4 mK. Pressure measurements are accurate to 0.002 MPa. The apparatus is fully automated.

We have verified the performance of the apparatus with measurements of carbon dioxide and propane vapor pressures. The data show that the isochoric apparatus has 0.07% accuracy in measuring pure component vapor pressures. The cross-checks show that the isochoric data is consistent with the temperature, pressure and density data from magnetic suspension densimeter within ± 0.1%.

Densities and phase boundaries have been determined for four gas mixtures. The densities are accurate to better than ± 0.1% over the entire range and dew points measurement accuracies are better than 0.5 K in temperature and 0.2% in pressure. The data from these four samples show that cubic equations of state, such as Peng-Robinson and Soave-Redich-Kwong have 1-20% errors in predicting hydrocarbon mixture dew points. The data also show that the AGA 8-DC92 equation of state has errors as large as 0.6% when predicting hydrocarbon mixture densities when its normal composition range is extrapolated. A new and better equation of state is needed in the natural gas industry for gas exploration, production and custody transfer.

We have the following recommendations concerning this research work. First, a good stirring mechanism for the fluid inside the cell should be designed and implemented. This should allow faster and better remixing when phase separation occurs. Second, the diffusion pump in the vacuum system should be replaced by a turbo molecular pump. Clean operations and reduced pump-down times are some of the advantages of turbo-molecular pumps. The operating cost of a turbo-molecular pump system is much less than a diffusion-pump system that requires a liquid nitrogen cold trap. Third, we recommend installing a separate, independent temperature sensor (thermocouple or RTD) and relay in the temperature measurement and control system to improve the safety features of the isochoric apparatus. This relay can shut down the entire system when the apparatus temperature exceeds a predetermined limit. This is very important if the apparatus is left unattended for a long period of time, *e.g.* overnight. Finally, a relief valve should be employed in the pressure system. No overpressure protection exists in the current pressure measurement system in order to maintain pressure measurement accuracy (the relief valve introduces a huge dead volume in the pressure measurement system). The new design should ensure that the relief valve temperature is controlled at the same temperature as the isochoric cell so its use would not reduce the pressure measurement accuracy.

NOMENCLATURE

B_k = Virial coefficients

C_v = Specific heat

e = Input error signal to the controller

K_c = Proportional gain of the controller

h = Sensor dissipation constant

I = Current

m_s = True mass of the sinker

m_s^* = Apparent mass of the sinker

PV = Process variable

R = Universal gas constants

R_R = Standard resistor for temperature measurement

S = Seebeck coefficient

SP = Setpoint

P = Pressure

t = Time

T = Temperature

T_i = Integral time

T_d = Reset time

T_{ref} = Reference temperature

V = Cell volume

V_s = Sinker volume

Z = Compressibility factor

Greek Letters

ρ = Density

γ = materials pressure coefficient

β = materials thermal coefficient

LITERATURE CITED

Benton, A. J., "Dew Point Measurement," *Hydrocarbon Engineering*, **7**, 59 (2002).

Bouchot, C., and D. Richon, "An Enhanced Method to Calibrate Vibrating Tube Densimeters," *Fluid Phase Equilibria*, **191**, 189 (2001).

Burnett, E. S., "Compressibility Determinations without Volume Measurement," *J. Appl. Mech*., **58**, A136 (1936).

Danesh, A., *PVT and Phase Behaviour of Petroleum Reservoir Fluids*, Elsevier, New York (1998).

Deters, U., and G. Schneider, "High Pressure Phase Equilibria: Experimental Methods," *Fluid Phase Equilibria*, **29**, 145 (1986).

Diller, D. E., "The Specific Heats (Cv) of Dense Simple Fluids," *Cryogenics*, **11**, 186 (1971).

Duarte-Garza, H.A., J. C. Holste, K. R. Hall, K. N. Marsh and B. E. Gammon "Isochoric PVT and Phase Equilibrium Measurements for Carbon Dioxide+Nitrogen," *Journal of Chemical and Engineering Data*, **40**,704 (1995).

Eubank, P. T., K. R. Hall, and J. C. Holste, "A Review of Experimental Techniques for Vapor-Liquid Equilibria at High Pressures," *Phase Equilibria and Fluid Properties in the Chemical Industry: Proceedings, 2nd International Conference*, H. Knapp and S. I. Sandler, eds., Great Neck, NY 675 (1980).

Eubank, P. T., and M. A. Barrufet, "General Conditions of Collinearity at the Phase Boundaries of Fluid Mixtures," *AIChE. J*., **33**(11), 1882 (1987).

Fenghour. A, J. P. M. Trusler, and W. A. Wakeham, "Phase Behaviour and Density of Model Reservoir Fluids at High Temperature and Pressure," *Fluid Phase Equilibria*, **158 –160**, 783 (1999).

Frederick, G., G. Keyes, and W. A. Felsing, "The Equation of State for Liquids and Vapors. I. The Vapor Phase of Ethyl Ether," *J. Am. Chem. Soc*., **41**(4), 9 (1919).

Gas Research Institute, "Policy Implications of the GRI Baseline Projection of U.S. Energy Supply and Demand to 2015," *GRI Baseline*, **3**, 31(1999).

Goodwin, A. R. H., K. N. Marsh, and W. A. Wakeham., *Measurement of the Thermodynamic Properties of Single Phases*, 1st edition, IUPAC Elsevier Science, Boston (2003).

Goodwin, R. D., "Apparatus for Determination of Pressure Density Temperature Relations and Specific Heats of Hydrogen to 350 atm at Temperatures above 14 K," *J. Res. Nat. Bur. Stand*., **65C**, 231 (1961).

Johansen, J. J., "Redesign of an Isochoric Apparatus for P-V-T Studies," Undergraduate Fellows Thesis, Texas A&M University, College Station, TX (2001).

Kellerman, S. J., "Determination of Thermodynamic Properties of Natural Gas Mixtures by Direct and Indirect Methods," Ph.D. Dissertation, Texas A&M University, College Station, TX (1994).

Kleinrahm, R., and W. Wagner, "Measurement and Correlation of the Equilibrium Liquid and Vapor Densities and the Vapor-Pressure along the Coexistence Curve of Methane," *Journal of Chemical Thermodynamics*, **18**(8), 739 (1986).

Knapp, H., *Vapor-Liquid Equilibria for Mixtures of Low-boiling Substances*, Scholium International, Great Neck, NY (1982).

Lau, W-W. R., "A Continusously Weighted Pycnometer Providing Densities for Carbon Dioxide + Ethane Mixtures Between 240 and 350 K at Pressures Up to 35 MPa," Ph.D. Dissertation, Texas A&M University, College Station, TX (1986).

Lemmon, E. W., A. P. Peskin, M. O. McLinden, and D. G. Friend, *NIST Standard Reference Database 12: Thermodynamic and Transport Properties of Pure Fluids Version 5.0*, National Institute of Standards and Technology, Standard Reference Data Program, Gaithersburg, MD (2000).

Linsky, D., J. M. H. Levelt Sengers, and H. A. Davis "Semiautomated PVT Facility for Fluids and Fluids Mixtures" *Review of Scientific Instruments*, **58**(5), 817(1987).

Matabe, A., "Effects of Some Design Parameters on the Accuracy of 'Isochoric' Measurements," M.S. Thesis, Texas A&M University, College Station, TX (1999).

May, E. F., T. J. Edwards, A. G. Mann, C. Edwards and R. C. Miller, "Development of an Automated Phase Behavior Measurement System for Lean Hydrocarbon Fluid Mixtures, Using Re-entrant Rf/microwave Resonant Cavities," *Fluid Phase Equilibria*, **185**, 339 (2001).

Melvin, A., *Natural Gas: Basic Science and Technology*, Adam Hilger, Philadelphia, PA (1988).

Nicholas, J. V., D. R. White, *Traceable Temperatures: An Introduction to Temperature Measurement and Calibration*, Wiley, New York (1994).

Nicola, G. D., G. Giuliani, G. Passerini, F. Polonara and R. Stryjek, "Vapor Liquid Equilibrium (VLE) Properties of R-32+R-134a System Derived From Isochoric Measurements," *Fluid Phase Equilibria*, **153**, 143 (1998).

Paroscientific Product Manual, "The Advantages of Digiquartz Technology," Paroscientific Inc., Redmond, WA (2004).

Peng, D. Y., and D. B. Robinson, "A New Two-constant Equation of State," *Ind. Eng. Chem. Fundam.*, **15**, 59 (1976).

Starling, K. E., M. Klein and F. E. Little, "The Thermodynamic Properties of Natural Gas-Physical Properties," *International Congress of Gas Quality*, Groningen, The Netherlands (1986).

Starling, K. E., and J. L. Savidge, Transmission Measurement Committee Report 8, American Gas Society, Washington D.C. (1992).

Soave, G., "Equilibrium Constants from Modified Redlich-Kwong Equation of State," *Chemical Engineering Science*, **27**, 1197 (1979).

Stouffer, C. E., S. J. Kellerman, K. R. Hall, J. C. Holste, K. N. Marsh and B. E. Gammon, " Densities of Carbon Dioxide+Hydrogen Sulfide Mixtures from 220 K to 450 K at Pressures up to 25 MPa," *Journal of Chemical and Engineering Data*, **46**, 1309 (2001).

Straty, G. C., and A. M. F. Palavra, "Automated High-Temperature PVT Apparatus with Data for Propane," *J. Res. Nat. Bur. Stand.*, **89**(5), 375 (1984).

Twu, C. H., D. S. Wayne, and V. Tassone, "Getting a Handle on Advanced Cubic Equations of State," *Chemical Engineering Progress*, **11**, 58 (2002).

Wagner, W., K. Brachthauser, R. Kleinrahm, and H. W. Losch, " A New Accurate Single-Sinker Densitometer for Temperatures From 233 to 523 K at Pressures Up to 30 MPa," *International Journal of Thermophysics*, **16**, 399 (1995).

Ward, R. W., and R. B. Wiggins, "Quartz Pressure Transducer Technologies," http://www.quartzdyne.com, Quartzdyne Inc., Salt Lake City, UT (2004).

Warner Jr, H. R., E. E. Leamer, A. P. Spence, R. L. Bone, R. A. Hubbard, J. Bernos, and W. A. Kriel, "Hydrocarbon Dewpoint Determination of Lean Natural Gases," *80th Annual Convention Presentations*, Gas Processors Association, Tulsa, OK (2001).

Yurttas, L, J. C. Holste and K. R. Hall, "Semiautomated Isochoric Apparatus for P-V- T and Phase Equilibrium Studies," *Journal of Chemical and Engineering Data*, **39**, 418 (1994).

APPENDIX A

PRT CALIBRATION

The thermometer resistance (model XS9691) was measured at fixed temperature points defined by ITS-90 or by comparison to a calibrated platinum resistance thermometer traceable to the National Institute of Standards and Technology. Resistance is measured with an excitation current of 1mA. Temperature is derived from measured resistance as follows:

For temperatures below 273.16 K:

$$W_r(T) = W(T) - a_4 \times [W(T) - 1] - b_4 [W(T) - 1] \times \ln W(T) \qquad \text{(A-1)}$$

For temperature above 273.16 K:

$$W_r(T) = W(T) - a_8 \times [W(T) - 1] - b_8 \times [W(T) - 1]^2 \qquad \text{(A-2)}$$

where W(T) = R(T)/R(273.16K), $W_r(T)$ defines temperature according to the ITS-90 reference function and the coefficients a_4, b_4, a_8, b_8 are unique to each individual thermometer.

In the range 13.8033 K to 273.16 K, the reference function $W_r(T)$ is

$$T/273.16K = B_0 + \sum_{i=1}^{15} B_i \{([W_r(T)]^{1/6} - 0.65)/0.35\}^i \qquad \text{(A-3)}$$

For temperatures above 273.16 K, the reference function is

$$T - 273.15K = D_0 + \sum_{i=1}^{9} D_i \{([W_r(T)] - 2.64)/1.64\}^i \qquad \text{(A-4)}$$

All the coefficients and constant used in equations (A-1) to (A-4) appear in Table A-1.

Table A-1. Coefficients in Temperature Calibration Equation.

Coefficient	Value	Coefficient	Value
B_0	0.183324722	D_0	439.932854
B_1	0.24095303	D_1	472.418020
B_2	0.209108771	D_2	37.684494
B_3	0.190439972	D_3	7.472018
B_4	0.142648498	D_4	2.920828
B_5	0.077993465	D_5	0.005184
B_6	0.012475611	D_6	-0.963864
B_7	-0.032267127	D_7	-0.188732
B_8	-0.075291522	D_8	0.191203
B_9	-0.056470670	D_9	0.049025
B_{10}	0.076201285		
B_{11}	0.123893204	R (273.16 K)	99.48443
B_{12}	-0.029201193	a_4	-1.3649453e-04
B_{13}	-0.091173542	b_4	2.3253476e-03
B_{14}	0.001317696	a_8	-6.0087756e-04
B_{15}	0.026025526	b_8	3.0925631e-04

APPENDIX B

SECONDARY STANDARD RESISTOR CALIBRATION

JRL resistor model CH46T4-100 has a measured value of 99.9902 ohms at 3.00 mA DC with an uncertainty of 0.3 ppm. The reported uncertainty represents an expanded uncertainty expressed at approximately the 95% confidence level using the coverage factor of k=2. The reported uncertainty is valid only at the time of test and does not take into account the effects of voltage/current, humidity, long-drift, transportation or other factors that may affect the stability of this resistance standard.

This standard resistor was checked by comparing it to a standard resistor (Leeds & Northrup primary standard resistor Model 4210-B) while in air at 23.0 °C with an automatic current comparator resistance bridge (Measurement International Model No 6010B). All values expressed are in terms of the SI 1990 values of voltage and resistance and in terms of ITS-90. The resistor is calibrated against Leeds & Northrup Primary standard resistor (model 4210-B) using a Measurement International AC bridge (model 6010B).

APPENDIX C

THERMOPILE DATA

An equation was fit to the response of a copper constantan thermocouple, the Seebeck coefficient, as a function of temperature.

$$S = \sum_{i=0}^{2} a_i T^i \qquad \text{(C-1)}$$

where $a_0 = 7.1826, a_1 = 0.13959, a_2 = -8.9924 \times 10^{-5}$, S is the Seebeck coefficient, with unit of Volts/K, a_i come from a least squares fit and T is in Kelvin. The following tables show the Seebeck coefficient, the value calculated with the equation, the difference between the two values and the fit parameters.

Table C-1. Fit of the Seebeck Coefficient from 200 to 450 K

T (K)	S (μV/K)	S_{calc} (μV/K)	$S - S_{calc}$ (μV/K)
198.15	31.213	31.311	-0.098
223.15	33.889	33.854	0.035
248.15	36.397	36.284	0.113
273.15	38.741	38.602	0.139
298.15	40.671	40.807	-0.136
323.15	42.808	42.900	-0.092
348.15	44.870	44.881	-0.011
373.15	46.773	46.749	0.024
398.15	48.520	48.504	0.016
423.15	50.149	50.148	0.001
448.15	51.687	51.679	0.008

APPENDIX D

PRESSURE TRANSDUCER CALIBRATION COEFFICIENTS

The following coefficients and parameters were used for the pressure transducer (model 43K-101, pressure range 0 to 3000 psia) calculation. Temperature is calculated using equations (D-1) and (D-2)

$$U = X - U_0 \tag{D-1}$$

$$\text{Temperature} = Y_1 U + Y_2 U^2 + Y_3 U^3 \tag{D-2}$$

where X is temperature period (μsec), the coefficient U_0, Y_1, Y_2, Y_3 are shown in Table D-1. Pressure is calculated by combining equation (D-3), (D-4), (D-5), and (D-6).

$$C = C_1 + C_2 U + C_3 U^2 \tag{D-3}$$

$$D = D_1 + D_2 U \tag{D-4}$$

$$T_0 = T_1 + T_2 U + T_3 U^2 + T_4 U^3 + T_5 U^4 \tag{D-5}$$

$$\text{Pressure} = C\left(1 - \frac{T_0^2}{T^2}\right)\left(1 - D\left(1 - \frac{T_0^2}{T^2}\right)\right) \tag{D-6}$$

where T is the pressure period (μsec). The coefficients $C_1, C_2, C_3, D_1, D_2, T_1, T_2, T_3, T_4$ and T_5 are also in Table D-1.

Table D-1. Calibration Coefficient

Parameter	Value	Unit
U_0	5.817934	μsec
Y_1	-4083.942	psia/μsec
Y_2	-12975.99	deg C/μsec^2
Y_3	0	
C_1	-15159.56	psia
C_2	115.3330	psia/μsec
C_3	47275.42	psia/μsec^2
D_1	0.046903	
D_2	0	
T_1	30.07890	μsec
T_2	1.101615	μsec/μsec
T_3	60.68878	μsec/μsec^2
T_4	206.8456	μsec/μsec^3
T_5	0	

APPENDIX E

COMPUTER PROGRAM

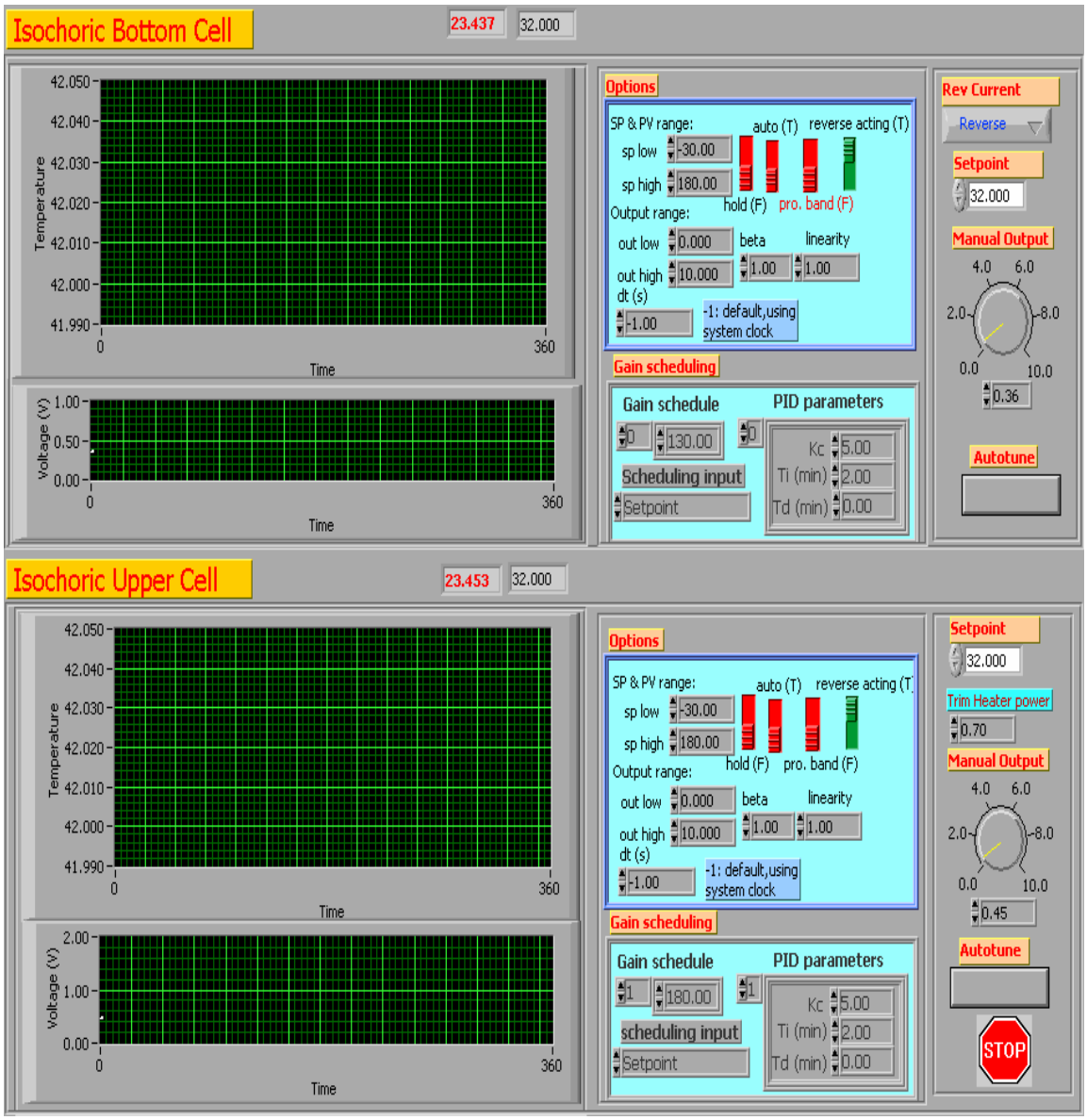

Figure E-1. Temperature measurement and control program (frontal panel).

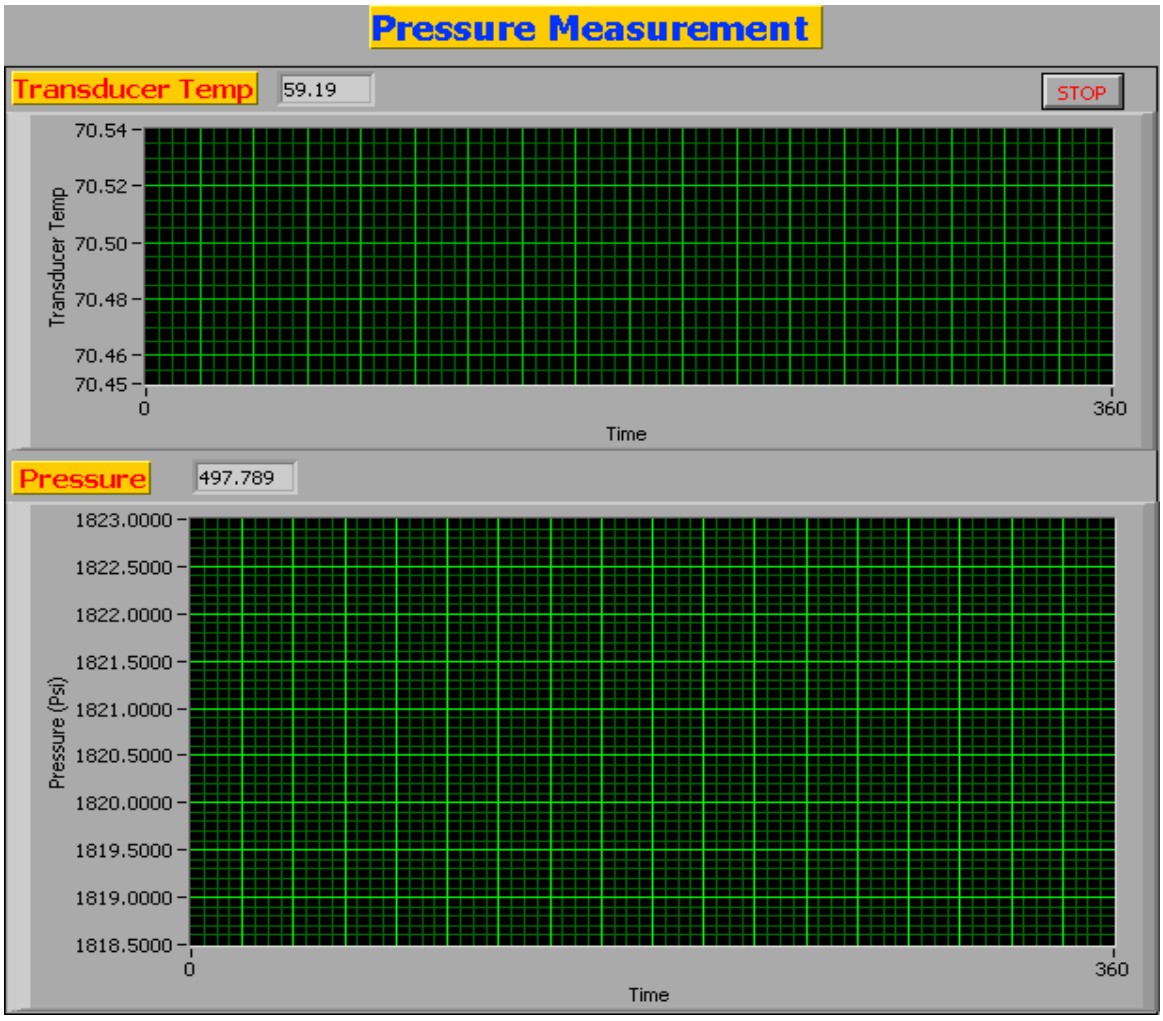

Figure E-2. Pressure measurement program (frontal panel).

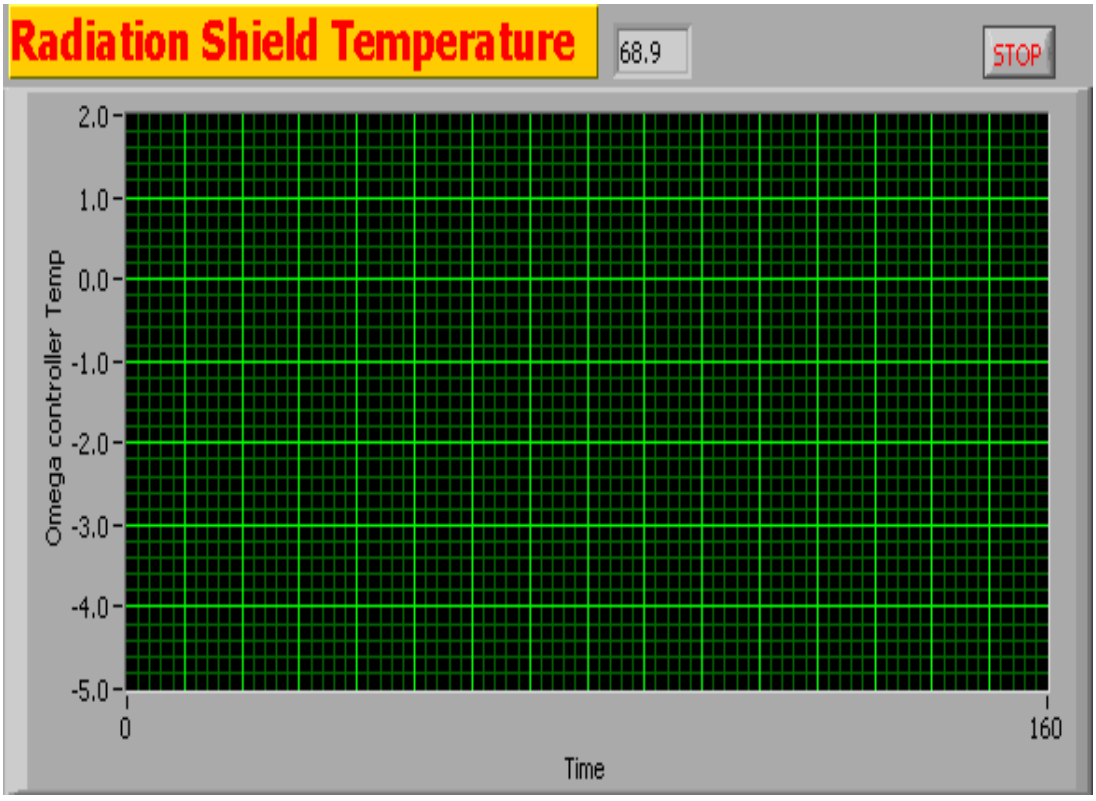

Figure E-3. Isothermal shield temperature measurement and control program (frontal panel).

APPENDIX F

91% METHANE GAS SAMPLE ISOCHORIC DATA

Table F-1. Isochore 1

Temp (K)	P_{exp} (psia)	P_{exp} (MPa)
305.15	2739.01	18.884808
290.65	2450.07	16.892637
270.15	2039.68	14.063097
236.45	1364.22	9.4059653
233.15	1298.61	8.9536004
230.15	1239.48	8.5459134
228.15	1200.18	8.2749494

Table F-2. Isochore 2

Temp (K)	P_{exp} (psia)	P_{exp} (MPa)
340.15	2851.53	19.660606
305.15	2311.37	15.936334
290.65	2084.56	14.372534
270.15	1761.75	12.146838
252.15	1476.23	10.178247
247.15	1396.84	9.6308723
243.15	1333.19	9.1920210
238.15	1253.83	8.6448531
236.15	1224.53	8.4428367

Table F-3. Isochore 3

Temp (K)	P_{exp} (psia)	P_{exp} (MPa)
340.15	2290.17	15.790166
305.15	1889.81	13.029780
290.65	1721.53	11.869531
270.15	1481.50	10.214582
260.15	1363.01	9.3976227
255.15	1303.65	8.9883499
250.15	1244.01	8.5771466
245.15	1189.20	8.199245
243.15	1168.23	8.0546619
241.15	1146.29	7.9033910

Table F-4. Isochore 4

Temp (K)	P_{exp} (psia)	P_{exp} (MPa)
340.15	1867.10	12.873201
305.15	1565.01	10.790363
290.65	1437.87	9.9137642
270.15	1255.99	8.6597458
260.15	1166.44	8.0423203
255.15	1122.26	7.7377099
250.15	1080.65	7.4508191
248.15	1064.16	7.3371246
247.15	1055.84	7.2797602

Table F-5. Isochore 5

Temp (K)	P_{exp} (psia)	P_{exp} (MPa)
340.15	1182.87	8.1556012
305.15	1018.59	7.0229305
290.65	949.470	6.5463649
270.15	850.656	5.8650664
265.15	826.515	5.6986201
262.15	812.275	5.6004387
258.15	793.055	5.4679215

Table F-6. Isochore 6

Temp (K)	P_{exp} (psia)	P_{exp} (MPa)
340.15	612.208	4.2210250
305.15	538.908	3.7156397
290.65	508.167	3.5036879
270.15	464.318	3.2013598
265.15	453.502	3.1267861
261.15	444.708	3.0661536
260.15	442.461	3.0506611
258.15	438.033	3.0201311

APPENDIX G

94% METHANE GAS SAMPLE ISOCHORIC DATA

Table G-1. Isochore 1

Temp (K)	P_{exp} (psia)	P_{exp} (MPa)
301.15	2797.49	19.288020
286.45	2482.22	17.114309
277.95	2298.48	15.847466
266.95	2061.29	14.212098
261.95	1953.51	13.468981
242.55	1537.28	10.599175
235.99	1396.01	9.625153
232.15	1326.41	9.145277
231.35	1311.90	9.045234

Table G-2. Isochore 2

Temp (K)	P_{exp} (psia)	P_{exp} (MPa)
301.15	2472.06	17.044258
287.75	2230.37	15.377864
279.95	2089.12	14.403979
267.95	1871.49	12.903473
261.95	1763.44	12.158494
247.42	1499.60	10.339381
242.55	1420.18	9.791799
238.55	1353.58	9.332608
237.45	1335.05	9.204848

Table G-3. Isochore 3

Temp (K)	P_{exp} (psia)	P_{exp} (MPa)
313.35	2369.67	16.338304
306.35	2264.93	15.616147
301.35	2189.93	15.099040
289.45	2011.10	13.866050
277.95	1836.72	12.663742
258.88	1545.80	10.657919
252.85	1462.55	10.083930
251.85	1448.44	9.986645
247.85	1391.77	9.595919
246.85	1377.34	9.496427

Table G-4. Isochore 4

Temp (K)	P_{exp} (psia)	P_{exp} (MPa)
333.35	2325.16	16.031418
323.35	2202.57	15.186190
313.35	2079.43	14.337169
303.35	1955.69	13.484011
290.45	1795.33	12.378368
284.45	1720.43	11.861950
277.15	1629.05	11.231907
274.15	1591.68	10.974250
270.15	1542.10	10.632408
270.14	1542.10	10.632408
267.15	1505.48	10.379922
263.15	1457.28	10.047595
260.15	1421.24	9.799107
257.15	1385.75	9.554412
256.15	1373.96	9.473123
254.45	1353.45	9.331712
253.45	1341.66	9.250422

Table G-5. Isochore 5

Temp (K)	P_{exp} (psia)	P_{exp} (MPa)
335.45	1794.16	12.370301
325.35	1709.35	11.785556
315.35	1624.88	11.203156
305.35	1540.01	10.617998
292.95	1434.33	9.889360
289.50	1404.00	9.680242
286.95	1383.31	9.537589
281.95	1341.20	9.247251
277.05	1300.20	8.964566
271.95	1257.51	8.670228
266.95	1215.84	8.382924

Table G-6. Isochore 6

Temp (K)	P_{exp} (psia)	P_{exp} (MPa)
335.45	1569.44	10.820911
327.05	1510.86	10.417016
320.15	1462.38	10.082758
313.15	1413.14	9.743260
305.15	1356.64	9.353706
294.97	1284.40	8.855629
292.95	1270.21	8.757792
287.95	1234.04	8.508409
281.95	1193.09	8.226068
277.05	1158.87	7.990129
271.95	1123.15	7.743849

Table G-7. Isochore 7

Temp (K)	P_{exp} (psia)	P_{exp} (MPa)
335.45	1379.92	9.514216
327.15	1331.25	9.178648
320.15	1289.98	8.894101
313.15	1248.56	8.608520
305.15	1201.12	8.281433
298.64	1162.30	8.013778
292.95	1128.77	7.782597
287.95	1099.25	7.579064
281.95	1063.82	7.334783
277.05	1034.95	7.135731
271.95	1004.77	6.927647

Table G-8. Isochore 8

Temp (K)	P_{exp} (psia)	P_{exp} (MPa)
335.45	1065.78	7.348296
327.15	1031.05	7.108841
320.15	1001.61	6.90586
313.15	972.078	6.702244
305.15	938.267	6.469125
303.71	932.15	6.42695
295.95	899.319	6.200588
292.95	886.657	6.113286
287.95	865.434	5.966959
281.95	839.992	5.791542
277.05	819.191	5.648125

Table G-9. Isochore 9

Temp (K)	P_{exp} (psia)	P_{exp} (MPa)
335.45	513.753	3.542203
327.15	499.337	3.442808
320.15	487.133	3.358665
313.15	474.869	3.274107
305.15	460.813	3.177195
304.52	459.660	3.169245
295.95	444.550	3.065065
292.95	439.241	3.028461
287.95	430.344	2.967118
281.95	419.608	2.893096

Table G-10. Isochore 10

Temp (K)	P_{exp} (psia)	P_{exp} (MPa)
335.45	216.590	1.493336
327.15	211.002	1.454808
320.15	206.284	1.422278
313.15	201.536	1.389542
305.15	196.102	1.352076
294.03	188.47	1.299455
287.95	184.307	1.270752
281.95	180.164	1.242187
277.05	176.766	1.218759
271.95	173.213	1.194262

APPENDIX H

88% METHANE GAS SAMPLE ISOCHORIC DATA

Table H-1. Isochore 1

Temp (K)	P_{exp} (psia)	P_{exp} (MPa)
302.05	2628.64	18.184307
287.65	2316.47	17.099209
280.65	2164.65	15.741218
274.65	2034.37	14.381226
270.65	1948.08	13.292544
255.5	1619.78	11.459228
250.65	1520.91	10.680809
248.65	1481.34	10.309458
247.65	1462.15	10.189489

Table H-2. Isochore 2

Temp (K)	P_{exp} (psia)	P_{exp} (MPa)
311.15	2637.41	18.184307
303.15	2480.03	17.099209
293.15	2283.07	15.741218
283.15	2085.82	14.381226
275.15	1927.92	13.292544
261.7	1662.02	11.459228
255.65	1549.12	10.680809
252.65	1495.26	10.309458
251.65	1477.86	10.189489
250.65	1460.34	10.068693

Table H-3. Isochore 3

Temp (K)	P_{exp} (psia)	P_{exp} (MPa)
320.15	2453.78	16.918222
308.35	2262.81	15.601530
302.15	2162.10	14.907159
293.15	2015.75	13.898111
283.15	1852.57	12.773024
273.0	1686.47	11.627804
264.65	1557.40	10.737898
262.65	1527.09	10.528918
260.65	1497.52	10.325040
259.65	1482.49	10.221411

Table H-4. Isochore 4

Temp (K)	P_{exp} (psia)	P_{exp} (MPa)
328.95	2268.35	15.639727
320.15	2151.28	14.832557
308.15	1991.31	13.729603
302.65	1917.41	13.220080
293.15	1789.57	12.338654
284.4	1671.30	11.523211
273.15	1526.04	10.521678
271.15	1500.98	10.348896
270.15	1488.33	10.261677

Table H-5. Isochore 5

Temp (K)	P_{exp} (psia)	P_{exp} (MPa)
338.95	2089.13	14.404048
328.95	1980.41	13.654450
320.15	1884.42	12.992622
308.15	1752.8	12.085134
300.15	1664.42	11.475775
293.6	1591.93	10.975974
285.15	1501.5	10.352481
281.15	1459.41	10.062280
279.15	1438.40	9.917421
278.15	1428.01	9.845785

Table H-6. Isochore 6

Temp (K)	P_{exp} (psia)	P_{exp} (MPa)
326.15	1483.25	10.226651
322.15	1453.97	10.024773
318.15	1425.82	9.830685
314.15	1395.35	9.620602
310.15	1365.99	9.418172
305.4	1329.99	9.169961
296.15	1264.13	8.715872
291.15	1228.07	8.467247
288.15	1206.45	8.318182
285.15	1184.79	8.168842

Table H-7. Isochore 7

Temp (K)	P_{exp} (psia)	P_{exp} (MPa)
335.15	1351.42	9.317715
332.15	1333.41	9.193541
328.15	1309.31	9.027377
324.15	1285.15	8.860800
320.15	1260.9	8.693602
308.8	1191.68	8.216347
303.05	1157.2	7.978615
300.15	1139.93	7.859543
296.15	1115.86	7.693586
292.15	1091.97	7.528870

Table H-8. Isochore 8

Temp (K)	P_{exp} (psia)	P_{exp} (MPa)
335.15	1175.81	8.106927
332.15	1160.92	8.004264
328.15	1141.01	7.866989
324.15	1121.06	7.729439
320.15	1101.09	7.591750
310.7	1053.73	7.265215
303.15	1015.89	7.004317
300.15	1000.95	6.901309
297.15	985.942	6.797833
293.15	965.952	6.660006

Table H-9. Isochore 9

Temp (K)	P_{exp} (psia)	P_{exp} (MPa)
342.45	849.336	5.855967
329.15	807.193	5.565401
325.15	794.609	5.478638
321.15	781.968	5.391481
316.15	766.136	5.282323
313.0	756.29	5.214437
310.15	747.058	5.150785
306.15	734.353	5.063187
301.65	720.010	4.964295
297.15	705.596	4.864914

Table H-10. Isochore 10

Temp (K)	P_{exp} (psia)	P_{exp} (MPa)
332.15	259.251	1.787473
329.15	256.745	1.770195
325.15	253.398	1.747118
321.15	250.039	1.723959
317.15	246.659	1.700654
310.15	240.788	1.660175
305.0	236.440	1.630197
306.15	237.403	1.636836
301.65	233.582	1.610492
297.15	229.737	1.583981

APPENDIX I

78% METHANE GAS SAMPLE ISOCHORIC DATA

Table I-1. Isochore 1

Temp (K)	P_{exp} (psia)	P_{exp} (MPa)
310.15	2788.38	19.225208
305.15	2658.07	18.326752
290.15	2268.97	15.644002
280.15	2012.68	13.876944
275.15	1885.80	13.002137
270.15	1761.03	12.141878
265.15	1638.91	11.299890
262.15	1567.84	10.809879
259.15	1501.50	10.352481
257.15	1467.75	10.119783

Table I-2. Isochore 2

Temp (K)	P_{exp} (psia)	P_{exp} (MPa)
330.15	2806.05	19.347039
310.15	2385.48	16.447310
305.15	2280.24	15.721705
290.15	1964.93	13.547719
285.15	1861.19	12.832457
280.15	1758.17	12.122159
275.15	1656.29	11.419721
270.15	1568.35	10.813395
268.15	1535.96	10.590074
265.15	1491.30	10.282154

Table I-3. Isochore 3

Temp (K)	P_{exp} (psia)	P_{exp} (MPa)
345.15	2633.44	18.156934
340.15	2550.05	17.581980
330.15	2383.00	16.430211
310.15	2048.41	14.123293
305.15	1964.51	13.544823
300.15	1880.80	12.967663
295.15	1796.51	12.386504
290.15	1713.26	11.812515
285.15	1632.94	11.258728
280.15	1563.63	10.780852
275.15	1498.26	10.330142

Table I-4. Isochore 4

Temp (K)	P_{exp} (psia)	P_{exp} (MPa)
345.15	2095.24	14.446175
340.15	2035.30	14.032903
330.15	1914.88	13.202636
320.15	1793.91	12.368577
310.15	1672.42	11.530933
305.15	1611.75	11.112628
300.15	1553.22	10.709078
296.15	1509.61	10.408397
293.15	1478.20	10.191833
290.15	1447.21	9.978164

Table I-5. Isochore 5

Temp (K)	P_{exp} (psia)	P_{exp} (MPa)
345.15	1612.23	11.115937
340.15	1571.26	10.833459
330.15	1489.49	10.269675
320.15	1407.03	9.701133
315.15	1366.18	9.419482
313.15	1350.02	9.308063
310.15	1327.13	9.150242
305.15	1288.89	8.886586

Table I-6. Isochore 6

Temp (K)	P_{exp} (psia)	P_{exp} (MPa)
345.15	1166.62	8.043564
340.15	1141.05	7.867265
335.15	1115.31	7.689794
330.15	1089.62	7.512667
325.15	1063.92	7.335472
320.15	1038.37	7.159311
317.15	1023.19	7.054649
315.15	1013.05	6.984736

Table I-7. Isochore 7

Temp (K)	P_{exp} (psia)	P_{exp} (MPa)
345.15	795.153	5.482388
340.15	779.887	5.377133
335.15	764.524	5.271209
330.15	749.154	5.165236
325.15	733.725	5.058857
321.15	721.311	4.973266
318.15	711.985	4.908965
315.15	702.573	4.844072

Table I-8. Isochore 8

Temp (K)	P_{exp} (psia)	P_{exp} (MPa)
345.15	557.335	3.842691
340.15	547.498	3.774867
335.15	537.677	3.707153
330.15	527.816	3.639164
325.15	517.876	3.570630
321.15	509.86	3.515362
318.15	503.803	3.473600
315.15	497.703	3.431542
312.15	491.574	3.389284

VITA

Jingjun Zhou was born in Zhejiang Province, P.R. China. He received the degrees of Bachelor of Science in chemical engineering in July 1996 and Master of Science in polymer science and engineering in April 1999 from Zhejiang University, China. In August 2000, he enrolled in the Ph.D. program in the chemical engineering department of Texas A&M University. He can be reached at: Daqitan No72, Jiangshan City, Zhejiang Province, P. R. China, 324123.